STRAINED EMPIRICAL PSEUDOPOTENTIAL GENERATION FROM HYBRID DENSITY FUNCTIONALS: GaAs, InAs, GaSb, InSb

A THESIS SUBMITTED TO

THE GRADUATE SCHOOL OF ENGINEERING AND SCIENCE

OF BILKENT UNIVERSITY

IN PARTIAL FULFILLMENT OF THE REQUIREMENTS FOR

THE DEGREE OF

MASTER OF SCIENCE

IN

DEPARTMENT OF PHYSICS

By

Aslı Çakan

August, 2015

Strained empirical pseudopotential generation from hybrid density functionals: GaAs, InAs, GaSb, InSb
By Aslı Çakan
August, 2015

We certify that we have read this thesis and that in our opinion it is fully adequate, in scope and in quality, as a thesis for the degree of Master of Science.

Assoc. Prof. Dr. Ceyhun Bulutay (Advisor)

Prof. Dr. Oğuz Gülseren

Assoc. Prof. Dr. Cem Sevik

Approved for the Graduate School of Engineering and Science:

Prof. Dr. Levent Onural
Director of the Graduate School

ABSTRACT

STRAINED EMPIRICAL PSEUDOPOTENTIAL GENERATION FROM HYBRID DENSITY FUNCTIONALS: GaAs, InAs, GaSb, InSb

Aslı Çakan
M.S. in Department of Physics
Advisor: Assoc. Prof. Dr. Ceyhun Bulutay
August, 2015

Self-assembled quantum dots composed of III-V compounds receive considerable attention due to their potential applications on spintronics and quantum information processing. Here, lattice mismatch between two materials causes a remarkable strain and this subsequently affects not only carriers but also nuclear spins due to electric quadrupole interaction. In this thesis, the behavior of electronic band structure and deformation potentials under various strains are investigated in the family of semiconductors consisting of InAs, GaAs, InSb and GaSb. Computations are performed using semi-empirical pseudopotential method (EPM) by generating a new set of strain-compliant pseudopotentials. In order to both lead and validate EPM calculations, density functional theory based on hybrid functionals has been employed. Our results on hydrostatic and shear strain deformation potentials obtained by either technique are in very good agreement with the experimental data. We demonstrate that the newly proposed empirical pseudopotentials perform well around band edges under anisotropic crystal deformations. This paves the way for large-scale electronic structure computations involving lattice mismatched constituents.

Keywords: Deformation potential, anisotropic strain, electronic band structure, empirical pseudopotential method, density functional theory, hybrid functionals.

ÖZET

HİBRİT YOĞUNLUK FONKSİYONELLERİNDEN GERİNMELİ YARI DENEYSEL GÖRÜNÜR POTANSİYEL ÜRETİMİ: GaAs, InAs, GaSb, InSb

Aslı Çakan
Fizik Bölümü, Yüksek Lisans
Tez Danışmanı: Doç. Dr. Ceyhun Bulutay
Ağustos, 2015

III-V bileşiklerinden oluşan ve kendiliğinden birleşen kuantum noktaları, olası spintronik ve kuantum bilişim teknoloji uygulamalarından dolayı artan ilgi görmektedir. Burada, her iki malzeme arasındaki örgü sabit farkı, ciddi gerinme alanına yol açmakta, ve bu durum dörtkutup çiftleniminden dolayı yalnızca taşıyıcıları değil, aynı zamanda çekin spinlerini de etkilemektedir. Bu çalışmada, GaAs, InAs, GaSb ve InSb yarıiletkenlerinin, çeşitli gerinmeler altındaki elektronik bant yapıları ve biçimsizlenme potansiyellerinin nasıl davrandığı araştırılmıştır. Hesaplamalar için yeni ürettiğimiz, gerinmeye duyarlı ve güvenilir yarı deneysel görünür potansiyeller kullanılmıştır. Bunlara hem yol gösterici olması, hem de desteklemek amacıyla, yoğunluk fonksiyoneli kuramına dayalı hibrit fonksiyonellerinden faydalanılmıştır. Hidrostatik ve makas gerinimine ait biçimsizlenme potansiyel hesaplamalarımız, her iki yöntemle de deneysel çalışmalarla oldukça uyumlu sonuçlar vermiştir. Yeni geliştirilen yarı deneysel görünür potansiyeller ile eşyönsüz kristal biçimsizlenme altında, bant kenarları etrafında oldukça iyi sonuçlar alındığı gösterilmiştir. Bu çalışma sayesinde, uyumsuz örgü sabitli malzemelerin büyük ölçekli elektronik yapı hesaplamalarına önemli bir zemin hazırlanmıştır.

Anahtar sözcükler: Biçimsizlenme potansiyeli, eşyönsüz gerinme, elektronik yapı hesabı, yarı deneysel görünür potansiyel yöntemi, yoğunluk fonksiyonel kuramı, hibrit fonksiyonelleri.

Acknowledgement

I would like to express my deepest gratitude to my advisor, Assoc. Prof. Dr. Ceyhun Bulutay, for his support, encouragement, patience and understanding throughout my graduate study. I cannot find any possible way to truly express my thanks to him for giving me a chance to work in his group.

I would like to acknowledge the members of my Thesis Committee, Prof. Dr. Oğuz Gülseren and Assoc. Prof. Dr. Cem Sevik, for kindly sparing their valuable times. I am grateful to Assoc. Prof. Dr. Cem Sevik for his encouragements and valuable suggestions concerning my DFT calculations. Without his help, this thesis would not materialize.

This thesis is an outgrowth of the TÜBİTAK under Project No:112T178, through which my fellowship has been granted in the last two years. The numerical calculations reported in this thesis were partially performed at TÜBİTAK ULAKBIM, High Performance and Grid Computing Center (TRUBA resources).

I acknowledge with much appreciation my colleague, Dr. Ümit Keleş, for many valuable discussions as well as in helping considerably with the technical issues. It has been a pleasure for me to have a chance to work with him in the same group.

I would like to thank to my officemates, Tuğba Andaç and Onur Tosun, for their unique friendship and support. My sincere thanks to my friends, Özlem Yeğrek, Pınar Telli, Olli Ahlstedt, Tayeb Bentria, Tomáš Bzdušek, Sevil Sarıkurt, Melis Beren Özer, Fulya Koç, Nur Kaynar and Aptullah Kahraman, for their contributions to the various domains and I greatly value their friendship.

I am indebted to my parents, Kemal and Hatice, my brother, Serhad, for their great understanding and support during my studies. This thesis would not have been possible without their support. I deeply appreciate them for encouraging me to follow my dreams and their belief in me.

Contents

List of Figures

List of Tables

Chapter 1

Introduction

Self-assembled heterostructures, such as InAs/GaAs and InSb/GaSb quantum dots, have been under the spotlight due to their potential application in future quantum computers or efficient quantum dot (QD) lasers or qubits [6, 7, 8]. Growth of self-assembled QDs occurs in the presence of the strain effects due to the lattice misfit at the interfaces of two different semiconductor materials [9, 10]. This pseudomorphic deformation is an important factor determining the electronic and optical features of self-assembled QDs.

Within the context of strain, the key concept of deformation potentials were introduced quite early by the fathers of semiconductor physics, Bardeen and Shockley [11] in 1950's for uniformly strained silicon and germanium which was generalized to many valley case by Herring and Vogt [12]. Next, Sham has worked out the shear deformation parameters related to the conduction band edge for Si in the framework of a pseudopotential rigid ion model [13]. In the 1960's, both conduction and valence band deformation potentials of Si under hydrostatic and uniaxial stress have been studied using self-consistent perturbation theory by Kleinman [14]. Subsequently, Ge and GaAs crystals under uniaxial strain have been investigated to define splitting of valence band and the direct band gap energy shift within optical reflection measurements by Balslev [15]. Shortly afterwards, the effect of uniaxial stress along [001], [110] and [111] on the electronic

structure of Ge, GaAs and Si was investigated by Pollak and Cardona with the calculation of hydrostatic and shear deformation potentials for both conduction and valence bands [16]. The decade of 1970's was quite stagnant for studies on deformation potentials except Pollak's experimental work on uniaxial deformed GaAs [17] and pioneering monograph of Bir and Pikus on strain-induced effects in semiconductors [18].

Revival period has started with Landolt-Börnstein experimental data compilation work for III-V semiconductors in 1980's [19]. Afterwards, theoretical attempts started to appear in the form of *ab initio* [20, 21, 22, 23, 24, 25, 9, 26] and semi-empirical methods [27, 28, 29, 1, 30, 3, 2]. Since *ab initio* calculations suffer from well-known band gap errors and require high computational cost [31], semiempirical methods have also been preferred [32]. In the same period, O'Reilly using tight-binding method has taken into account the crystals under biaxial compression and tension to study [001] axial deformation potential b in group III-V semiconductors [33]. It has been shown that in biaxially strained materials, the heavy hole band could show light-hole type characteristic [29]. As a matter of fact, this result has ramifications in quantum information science and technology which is also supported by recent works performed by Kim and Fischietti [3], Bester and Cardenas [7].

In 1999, Zunger and Meyer fitted [34] their pseudopotential on deformation potentials based on first-principle local density approximation (LDA) calculations. They emphasize that the given deformation parameters in the literature varies in a range and cannot be fitted explicitly. More recently, a comprehensive compilation has been carried out by Vurgaftman and Meyer due to demand for up to date reliable semiconductor data [5]. Inevitably, they express the deformation potentials as ranges and give recommendations which are ambiguous for some materials. Notably, there are experimental discrepancies on b and d biaxial deformation potentials. Therefore, the necessity for reliable deformation potentials for common III-V semiconductors is still a pressing issue within the community.

Computation of the electronic structure of solids has been one of the main challenges since the development of quantum mechanics in 1920's and 1930's

[35]. The major step for interpreting of electronic features of solids was in 1960's, developing a useful empirical approach to describe the electron-core and electron-electron interactions. This advancement was primarily lead by Marvin Cohen for the purpose of producing accurate band structures as fitting a few parameters to optical data in 1980's [36, 37] which is called empirical pseudopotential method (EPM). It gives accurate information about the electronic properties of solids within a modest computational budget [27, 28, 29, 1, 30, 3, 2].

On the other hand, over the last decade, density functional theory (DFT) calculations with hybrid functionals have gained increasing attention as they offer a remedy for the well-known LDA failures with the approach by Heyd-Scuseria-Ernzerhof (HSE) [38]. HSE functionals basically combine LDA or Generalized gradient approximation (GGA) exchange-correlation functionals with Hartree-Fock (HF, exact) exchange. One of the most advantageous features of HSE is to use conventional *local* functional instead of long-range part of HF term, however, short-range part is switched to the non-local HF potential since the calculation of long-range part for localized basis sets (Projected augmented wave-PAW) is troublesome and computationally costly. So that, HSE reduces the high cost of hybrid functionals which is twice of conventional LDA or GGA functionals and provides much reliable energy band gaps for III-V materials. Hence, it is well suited as an efficient method for studies on strained materials. As a matter of fact, Walle *et. al.* have calculated shear deformation potentials of GaN and InN to explore the effect of strain in polarization switching in InGaN/GaN quantum wells using HSE06 functional [39]. GaN and InN wurtzite phases within AlN, ZnO [40], InAs and InP [41] have been employed to obtain complete sets of deformation potentials for reasonable strain conditions in the linear regime around the experimental equilibrium volume comparing HSE06 and G_0W_0 based calculations.

1.0.1 This Work

In this work, due to the aforementioned issues regarding strained semiconductors and because of the fact that among the Group III-V semiconductors, GaAs, InAs,

GaSb and InSb span the widest direct gap energy [42], we have aspired to investigate the electronic properties of these materials under different deformations by theoretical/computational methods. We choose two approaches; empirical pseudopotential method (EPM) and *ab initio* methods. In Chapter 2, our attempt is to look for the efficient and reliable ways to obtain satisfying results on the electronic structure calculations using the latest hybrid functional based technique. Among various alternatives, we opt for HSEsol functional which is based on one of the GGA types called PBEsol [43, 44] due to the assertion that it gives satisfying results for small gap semiconductors [45]. In the light of these reliable first-principles results, we propose a new EPM parametrization. In Chapter 3, we report our extensive comparative studies on the band structure of strained materials and, conclude in Chapter 4 with possible extensions of this work and potential applications of self-assembled QDs in the field of spintronics and quantum information processing.

Chapter 2

Theoretical Framework: EPM and DFT

The total Hamiltonian for a given crystal typically includes kinetic energies of the electron and cores, electron-electron, core-core, and electron-core Coulomb interactions with the relativistic effects [35]. However, practically, it is not possible to account for all the interactions in the crystal. Therefore, multifarious approximations are employed to solve this problem [46];

- One of them is to divide electrons into two parts as valence and core electrons.
- The other one is to suppose the ions as stationary.
- Yet another is to assume that each electron experiences the same average potential (known as mean-field approximation).

So that, the many-body Hamiltonian reduces to the one-particle Hamiltonian as follows;

$$H\psi = \left[-\frac{\hbar^2}{2m_0}\nabla^2 + V_{lat}(\mathbf{r})\right]\psi = E\psi, \tag{2.1}$$

where m_0 is the free electron mass, ψ is the true wave function and $V_{lat}(\mathbf{r})$ is the crystal potential that represents electron-electron and electron-core interactions [47, 48]. Due to the fact that these interactions are taken as averaged, each electron moves in this average potential [37]. Now, the calculation has two steps; first one is the determination of the one-electron potential and second one is the determination of a convenient way to solve this eigenvalue problem. It can be solved by *ab initio* methods where $V_{lat}(\mathbf{r})$ is calculated with atomic positions and atomic numbers as the only input parameters or by EPM that is expressed in terms of parameters determined by fitting experimental data.

2.1 Empirical Pseudopotential Method

In the framework of EPM, because of the fact that our interest is related to the calculation of electronic band structure parameters, we can further simplify the problem by neglecting the core vibration and assuming fixed cores. In the core region, the crystal potential, V_{lat}, is a highly varying function of the real space in order to maintain the orthogonality with the core states. The rapid oscillation of the true wave functions puts difficulties to solve the problem. In order to overcome this issue, pseudopotential concept suggests to separate the wave function into two parts as a smooth (pseudo-wave function) and oscillatory part. The kinetic energies from the oscillatory part provide an effective repulsive potential for the valence electrons in the core region. By means of that, one can replace the true wave function, ψ, and potential by a smooth pseudo-wave function, ϕ, and a weaker effective "*pseudopotential*". In that sense, the Hamiltonian can be rewritten as follows:

$$H\phi = \left[-\frac{\hbar^2}{2m_0}\nabla^2 + V_{psp}\right]\phi = E\phi. \tag{2.2}$$

The Eq. (2.2) is called pseudopotential equation and we can obtain the correct pseudo-wave function, ϕ, outside cores. The energy E is identical to the eigenvalue corresponding to the exact wave function ψ and ϕ slowly varies in the core region in contrast to ψ [37]. With this approach, providing less oscillation in the

core region means the usage of lower cutoff energy to represent the orbitals, which brings very low memory requirement and fast computation.

At that stage, it can be simplified by the translational symmetry of the crystal. Hence, one can achieve a matrix form of the Hamiltonian by performing Bloch's theorem first and expanding the general solution over products of Bloch functions and plane waves. The one-electron Schrödinger equation;

$$\left[\frac{p^2}{2m_0} + V_{lat}(\mathbf{r})\right]\phi(\mathbf{r}) = E\phi(\mathbf{r}), \tag{2.3}$$

put to the periodic boundary condition $V(\mathbf{r}) = V(\mathbf{r} + \mathbf{R_n})$ has to be of the form;

$$\begin{aligned} \phi(\mathbf{r}) &= e^{i\mathbf{k}\cdot\mathbf{r}}u_{\mathbf{k}}(\mathbf{r}), \\ u_{\mathbf{k}}(\mathbf{r}) &= u_{\mathbf{k}}(\mathbf{r} + \mathbf{R_n}) \ . \end{aligned}$$

Due to the periodicity of the lattice of $u_{\mathbf{k}}(\mathbf{r})$, the expansion of a Fourier sum of it as follows;

$$u_{\mathbf{k}}(\mathbf{r}) = \sum_j A_j(\mathbf{k})e^{i\mathbf{G_j}\cdot\tau} \ ,$$

where, $\mathbf{G}_j$ are the reciprocal lattice vectors. Then the one-electron Schrödinger equation can be rewritten as;

$$\left[\frac{(p+\hbar k)^2}{2m_0} + V_{lat}(\mathbf{r})\right]u_{\mathbf{k}}(\mathbf{r}) = E_n(\mathbf{k})u_{\mathbf{k}}(\mathbf{r}) \ . \tag{2.4}$$

Here, we add the index of band n to $E_n(\mathbf{k})$ and $\phi_{n,\mathbf{k}}(\mathbf{r})$ to label the energy bands. Likewise, Fourier sum of $V_{lat}(\mathbf{r})$ is written according to the periodicity of the lattice;

$$\begin{aligned} V_{lat}(\mathbf{r}) &= \sum_{\mathbf{G}} V(\mathbf{G})e^{i\mathbf{G}\cdot\mathbf{r}} \ , \\ V(\mathbf{G}) &= \frac{1}{\Omega}\int e^{-i\mathbf{G}\cdot\mathbf{r}}V_{lat}(\mathbf{r})d\mathbf{r} \ , \end{aligned}$$

where, Ω is the cell volume. The crystal potential, $V_{lat}(\mathbf{r})$, is represented by a linear superposition of atomic potentials;

$$V_{lat}(\mathbf{r}) = \sum_{\mathbf{R},\tau} V_{ion}(\mathbf{r} - \mathbf{R} - \tau) \ , \tag{2.5}$$

$$V(\mathbf{G}) = \frac{1}{\Omega}\int_{\Omega}\sum_{\mathbf{R},\tau} V_{ion}(\mathbf{r}-\mathbf{R}-\tau)e^{-i\mathbf{G}\cdot\mathbf{r}}d\mathbf{r} \ ,$$

where V_{ion} is the ionic potential for the basis ion at τ in the cell at $\mathbf{R}$ and assuming the wave functions are normalized to the volume Ω of the crystal. Here, $\mathbf{R}$ is a lattice vector and τ denotes a basis vector. In the reciprocal lattice, expression of the potential is given as follows;

$$V_{lat}(\mathbf{G}) = \sum_{\mathbf{G}} V_{ion}(\mathbf{G})S(\mathbf{G})e^{i\mathbf{G}\cdot\mathbf{r}} \ , \tag{2.6}$$

where the structure factor is $S(\mathbf{G}) = \frac{1}{N_a}\sum_{\tau} e^{-i\mathbf{G}\cdot\tau}$, $V_{ion}(\mathbf{G})$ is the atomic form factor and N_a represents the number of basis atoms. The wave functions ,$\phi_{n,\mathbf{k}}(\mathbf{r})$, and the values of band energy, $E_n(\mathbf{k})$, are a result of;

$$\left[\frac{p^2}{2m_0} + V_{lat}(\mathbf{r})\right]\phi_{n,\mathbf{k}}(\mathbf{r}) = E_n(\mathbf{k})\phi_{n,\mathbf{k}}(\mathbf{r}) \ , \tag{2.7}$$

where $V_{lat}(\mathbf{r})$ is given by Eq. (2.6), $\phi_{n,\mathbf{k}}(\mathbf{r})$ has the Bloch form and they can be expanded in a set of plane waves. Hence, the required parameters for this calculation are only the structure factors and the atomic form factors.

According to the local pseudopotential approach, we can empirically fit atomic form factors to the experimental data to get correct band structure of valence electrons which plays a key role to the chemical or physical properties of the crystal [47, 48].

For the zinc-blende lattices, the potential, Eq. (2.6), takes the form of;

$$V(\mathbf{G}) = V_S(\mathbf{G})\cos\mathbf{G}\cdot\tau + iV_A(\mathbf{G})\sin\mathbf{G}\cdot\tau \ . \tag{2.8}$$

$V_S(\mathbf{G})$ is the sum of symmetric form factors and $V_A(\mathbf{G})$ is the differences of antisymmetric ones. They can be specialized for the diamond or zinc-blende compounds which have two ions in the unit cell at $\tau_\mathbf{1}$ =(0, 0, 0) and $\tau_\mathbf{2} = a_0(1, 1, 1)/4$ where a_0 is the unstrained lattice constant in Cartesian coordinates. In this case, the atomic form factor can be simplified as;

$$\begin{aligned} V(\mathbf{G}) &= V_1 e^{-i\mathbf{G}\cdot\tau_\mathbf{1}} + V_2 e^{-i\mathbf{G}\cdot\tau_\mathbf{2}}, \\ &= V_s(\mathbf{G})\underbrace{S_s(\mathbf{G})}_{\cos\mathbf{G}\cdot\tau} + iV_a(\mathbf{G})\underbrace{S_a(\mathbf{G})}_{\sin\mathbf{G}\cdot\tau} \ . \end{aligned}$$

$$V_s(\mathbf{G}) = \frac{1}{2}(V_1 + V_2),$$
$$V_a(\mathbf{G}) = \frac{1}{2}(V_1 - V_2).$$

Here, 1 and 2 indicate the anion (As, Sb, etc.) and cation (In, Ga, etc.), respectively, for zinc-blende crystals. Basically, EPM necessities the fit of $V(\mathbf{G})$'s to the experimental parameters and the assumption of the ionic potential as spherically symmetric (in its local version), the form factors are related to the magnitude of $\mathbf{G}$. In practice, we only need three form factors at $|\mathbf{G}| = \sqrt{3}, \sqrt{8}(\sqrt{4})$ and $\sqrt{11} \times (2\pi/a_0)$ since the full Fourier transform $V(q) = V(|\mathbf{G}|)$ becomes very weak for $|q|$ larger than $\sqrt{11} \times (2\pi/a_0)$ due to the elimination of the strong core potential.

Afterwards, we solve Schrödinger equation for the eigenvectors, $\phi_{n,\mathbf{k}}$, and eigenvalues, $E_{n,\mathbf{k}}$ through which we can readily extract the following properties:

- Energy band gap (E_{gap}) and effective mass (m^*),
- Hydrostatic (a_{gap})and shear (b and d) deformation potentials,
- Band offsets and spin-orbit splitting (Δ_{so}).

2.1.1 Searching among existing EPM parametrizations

In their work, Bester and Cárdenas [26] reproduce experimentally determined band energies by means of atomistic empirical pseudopotential method (AEPM) from LDA calculations. They use high values of plane wave energy cutoff ($\sim$ 80 Ry) and prefer to use the band gap energy at L point for InAs since it has a vanishing band gap in LDA. Unfortunately, this approach does not fulfill our demand due to their large values of plane wave energy cutoff as well as suffering from the well-known LDA band gap error.

Our next focus has been on Williamson *et. al.* work [1] which is completely based on EPM. They express $V(q)$ as given in Eq. (2.10) with the parameters

given in the Table 2.1. The kinetic energy is scaled by the factor β and their argument on it is that introducing such a scaling for the kinetic energy allows for a simultaneous fit of the energy gaps and the effective masses ($\beta = 1.23$ is used for both InAs and GAs).

Table 2.1: Fitting parameters given by Williamson *et. al.* [1] for InAs and GaAs pseudopotentials. 5 Ry plane wave cutoff is needed for the potentials.

Parameter	In	Ga	As (InAs)	As (GaAs)
a_0	644.13	432960	26.468	10.933
a_1	1.5126	1.7842	3.0313	3.0905
a_2	15.201	18880	1.2464	1.1040
a_3	0.35374	0.20810	0.42129	0.23304
γ_α	2.1821	2.5639	0.0	0.0

The local potential part is constructed including hydrostatic strain dependency with $\mathrm{Tr}(\varepsilon) = \varepsilon_{xx} + \varepsilon_{yy} + \varepsilon_{zz}$;

$$V_\alpha^{loc}(r;\varepsilon) = V_\alpha^{eq}(r;0)[1 + \gamma_\alpha \mathtt{Tr}(\varepsilon)] \ . \tag{2.9}$$

a_0, a_1, a_2, a_3 and γ_α are fitted to the experimental bulk properties of GaAs and InAs. Unstrained local pseudopotential $V_\alpha^{eq}(r;0)$ in reciprocal space q is given as:

$$V(q) = \frac{a_0(q^2 - a_1)}{a_2 e^{a_3 q^2} - 1} \ . \tag{2.10}$$

We can mention a similar pseudopotential proposed by He *et. al.* [2] subject to the same Eq. (2.10) with the parameters in Table 2.2.

We have followed the aforementioned parameters of Zunger's and He's group in our calculations. Our results on effective masses, spin-orbit splittings, direct and indirect energy gaps are in very good agreement with their calculations and experimental results. However, our main target is to obtain the deformation potentials under hydrostatic and uniaxial stresses due to the presence of various axial distortions in self-assembled QDs. Thus, we came to conclusion that the performance of these pseudopotentials fall short of our expectations under various kind of strains since they were developed originally at most for hydrostatic conditions.

Table 2.2: Fitting parameters given by He *et. al.* [2] for InAs and GaAs pseudopotentials. 5 Ry plane wave cutoff is needed for the potentials.

Parameter	In	Ga	As (InAs)	As (GaAs)
a_0	771.3695	476845.70	26.8882	11.9753
a_1	1.6443	1.9102	2.9716	3.0181
a_2	18.1342	22909.50	1.2437	1.1098
a_3	0.3940	0.1900	0.4276	0.2453
γ_α	2.1531	2.5215	0.0	0.0

Afterwards, with the prospect of achieving strain-compliant pseudopotentials, we turned to Kim *et. al.* [3] on electronic band structure for biaxially strained semiconductors based on EPM including both local and nonlocal parts with strain. They emphasize insufficiency of the local form factors when the strain comes into question. For this reason, they choose to employ an interpolation and put forward various interpolation patterns to fit deformation potentials to the experimental results besides band structure and effective masses. They utilize a cubic spline interpolation due to its advantages of giving a permission to control curve slopes at a given q with a q-dependent local pseudopotential presented as;

$$V(q) = V(q)_{cubic} \times \left[\frac{1}{2}\tanh\left\{\frac{a_5 - q^2}{a_6}\right\} + \frac{1}{2}\right], \tag{2.11}$$

where "tanh" part is introduced for a fast cutoff the pseudopotential at high q and $V(q)_{cubic}$ represents the cubic spline interpolation of the local form factors which consists of symmetric and antisymmetric components, $V^s(q)_{cubic}$ and $V^a(q)_{cubic}$. Here, a_5 and a_6 are fitting parameters.

By taking inspiration from this approach, we decided to follow the same form, however, without including the nonlocal part under the hope that only local empirical pseudopotential with the cubic spline interpolation can fulfill our demands. Consequently, aiming to construct a pseudopotential which has a high performance not only under hydrostatic strain, but also under the other type of strains such as uniaxial and biaxial along several directions by means of only local empirical pseudopotential. We retain the local potential part as hydrostatic strain dependent as given in Eq. (2.9) and take q-dependent local pseudopotential

as shown in Eq. (2.11). In other words, we combine the ideas arouse from the study of Zunger *et. al.* and Kim *et. al.* by taking Eq. (2.9) and Eq. (2.11) into account. Hence, for the purpose of exploring all of the axial deformations, our quest has ended up with introducing a new strain-performing pseudopotential with the parameters as given in Table 2.4 and 2.5. Also, we present the effective mass values for each material calculated with this new parametrization as shown in the Table (2.3).

Table 2.3: Effective masses (in m_0) at Γ point in k-space for conduction band ($m_e^{*\Gamma}$), heavy hole $m_{hh}^{*\Gamma}$, light hole $m_{lh}^{*\Gamma}$ and split-off $m_{so}^{*\Gamma}$ bands.

Material		$m_e^{*\Gamma}$	$m_{hh}^{*\Gamma}[001]$	$m_{hh}^{*\Gamma}[110]$	$m_{hh}^{*\Gamma}[111]$	$m_{lh}^{*\Gamma}[001]$	$m_{lh}^{*\Gamma}[110]$	$m_{lh}^{*\Gamma}[111]$	$m_{so}^{*\Gamma}$
GaAs	This work	0.082	0.439	0.845	1.143	0.111	0.099	0.096	0.218
	Ref. [3]	0.082	0.382	0.696	0.903	0.106	0.094	0.091	0.206
	Literature	0.063	0.388	0.658	0.920	0.089	0.081	0.079	0.33-0.388
GaSb	This work	0.054	0.363	0.724	1.027	0.066	0.060	0.059	0.20
	Ref. [3]	0.049	0.289	0.534	0.712	0.056	0.052	0.050	0.19
	Literature	0.041	0.23	–	0.57	–	0.05	–	0.14
InAs	This work	0.030	0.433	0.814	1.127	0.038	0.036	0.036	0.127
	Ref. [3]	0.026	0.31	0.547	0.720	0.032	0.03	0.03	0.109
	Literature	0.023	0.39	0.98	0.757	0.042	0.041	0.014	0.09-0.15
InSb	This work	0.022	0.357	0.714	1.049	0.024	0.023	0.023	0.172
	Ref. [3]	0.017	0.304	0.534	0.705	0.019	0.018	0.018	0.155
	Literature	0.014	0.26	–	0.68	0.015	0.015	–	0.19

Table 2.4: Compound-based fitted spin-orbit coupling parameters, λ (Ry). The detailed explanation and expressions are given in Appendix A.

Compound	λ
GaAs	0.02129
InAs	0.02049
GaSb	0.03854
InSb	0.0377

Table 2.5: Empirical local pseudopotential parameters. The form factors $V^{s,a}_{\sqrt{3}}$, $V^{a}_{\sqrt{4}}$, $V^{s}_{\sqrt{8}}$ and $V^{s,a}_{\sqrt{11}}$ (in Ry) for all four materials are tuned to fit experimental band gaps and deformation potentials, starting from the local EPM values reported in Ref. [3]. $V^{s,a}(q=0)$ is adjusted to Ref. [4] to line-up the natural valence band offsets.

		Material			
Quantity	Symbol	GaAs	InAs	GaSb	InSb
Local Form Factor	$V^{s}_{\sqrt{3}}$	-0.235	-0.207	-0.2043	-0.199
	$V^{s}_{\sqrt{8}}$	0.015	0.0	0.0	0.0115
	$V^{s}_{\sqrt{11}}$	0.0729	0.0465	0.06011	0.03341
	$V^{a}_{\sqrt{3}}$	0.076	0.054	0.033	0.0416
	$V^{a}_{\sqrt{4}}$	0.057	0.0466	0.028	0.035
	$V^{a}_{\sqrt{11}}$	0.0061	0.007	0.0054	0.006
Cubic spline interpolation parameters	$S^{s}_{\sqrt{3}}$	0.05673	-0.1913	-0.181	-0.1529
	$S^{s}_{\sqrt{8}}$	0.125	0.125	0.14	0.06059
	$S^{s}_{\sqrt{11}}$	0.05955	-0.00625	-0.0819	0.01
	$S^{a}_{\sqrt{3}}$	0.025	-0.035	-0.05	-0.05
	$S^{a}_{\sqrt{4}}$	-0.115	-0.09	-0.04	-0.04
	$S^{a}_{\sqrt{11}}$	-0.01	-0.022	-0.03	-0.03
	a_5 (a.u.)	4.05	4.5	4.0	3.9
	a_6 (a.u.)	0.39	0.41	0.3	0.3
	$V^{s}(0)$	-0.642	-0.546	-0.526	-0.424
	$V^{a}(0)$	-0.104	-0.088	-0.047	-0.045
Cutoff energy	$\mathrm{E_{cutoff}}$(Ry)	5.0	4.85	5.0	4.85

Table 2.6: Comparison of the direct gap, E_{gap}, and split-off gap (in eV), Δ_{so}, acquired from the empirical pseudopotential calculations and the experimental values [5]. In our EPM calculations, lattice constants are taken from Ref. [5].

Material		E_{gap}	Δ_{so}
GaAs	This Work	1.51	0.36
	Expt.	1.51	0.34
InAs	This Work	0.41	0.38
	Expt.	0.41	0.39
GaSb	This Work	0.81	0.72
	Expt.	0.81	0.76
InSb	This Work	0.23	0.76
	Expt.	0.23	0.81

In fitting the EPM, b and d deformation potentials for each material, we made use of extensive calculations from the DFT as described in detail in the following section.

2.2 DFT Calculations for GaAs, InAs, GaSb and InSb

DFT is a theory of electronic ground state property calculation for molecules and solids. This calculation is performed by means of Kohn-Sham (KS) formalism which constructs many-electron systems as non-interacting particle systems. By this approach, the density of the particles is allowed to be the same as in the real system. DFT with the solution of KS is an efficient quantum mechanical way to solve and find out of the material properties [31].

However, the problematic part arises from exchange-correlation interactions [49]. All exchange and correlation effects of many-electron systems are carried by exchange-correlation energy functionals and there is always need to approximate for these functionals. Choice of exchange correlation energy functional is one of the most important part which defines the accuracy of the DFT calculation.

LDA, GGA and hybrid functionals are the most frequently used approximations to solve that part.

2.2.1 Choice of Exchange-Correlation Energy Functional

LDA and GGA based functionals have yielded quite reliable results for many materials. However, these approaches express the density of exchange-correlation energy only as a function of local electron density and do not take into account non-local dependency. LDA (local) and GGA (semi-local) based functionals aim to solve exchange-correlation energies depending only on density and gradient of density, respectively. Therefore, we have started to explore electronic structures of strained materials using LDA and GGA based projector augmented wave (PAW) pseudopotentials. We have performed our calculations by aid of ABINIT software [50] and used the implemented pseudopotentials called JTH-LDA and JTH-PBE PAW data sets produced by Holwarth *et. al.* [51].

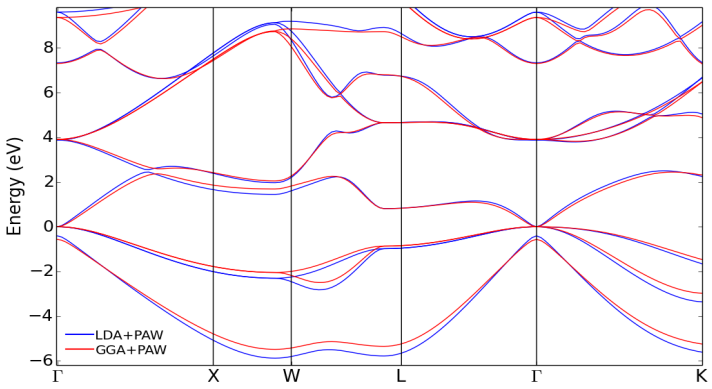

Figure 2.1: InAs band structure calculated by JTH-LDA and PBE PAW pseudopotentials (not including spin-orbit interaction). InAs shows a metallic behavior for these methods.

LDA and GGA based approaches bring inevitably systematical errors such as geometrical properties, atomization and surface energies. This issue is one of the most known problem of DFT calculations. Lattice parameter calculations with

Table 2.7: Lattice constant, bulk modulus and band gap energy values calculated by JTH-LDA and PBE PAW pseudopotentials for InAs.

Property	JTH-LDA PAW	JTH-PBE PAW	Expt.
Lattice Constant (Å)	6.065	6.022	6.058
B (GPA)	61.26	49	58
E_{gap} (eV)	metallic	metallic	0.42

common used LDA and GGA based Perdew-Burke-Ernzerhof PBE functionals have concluded with $\sim$ %1-2 error. Furthermore, metallic behavior is observed in both cases as shown Figure 2.1. Therefore, the reasons of LDA and GGA functionals' deficiency can be put in order as follows [49]:

- Interaction of total electron charge and an electron contains the interaction of the electron by itself which is unphysical and called as self-interaction. This extra term should be compensated adding a term which has an opposite sign but identical. However, cancelation of this term is unsuccessful so that some parts of this self-interaction term remain in the calculation.

- The other reason is that these functionals cause a discontinuity in exchange-correlation potential depending on change of particle number. Therefore, LDA and GGA functionals do not reflect the exact asymptotic behavior of exchange and correlation effects.

We concluded that LDA and GGA functionals are not satisfactory especially small band gap semiconductors that we deal with. Our calculations on GaAs by the same method supported that conclusion, as well.

With the hope to overcome those problems, we switched to the PAW+U method which "U" term increases and reorganizes energy band gap of between empty *3d* states and filled states. In other words, PAW+U is a LDA or GGA based calculation method which contains pairing with an additional orbital interaction [31]. This additional term causes localized orbital shifting, relatively to the others. This method aims to remove the aforementioned problems of LDA

and GGA functionals.

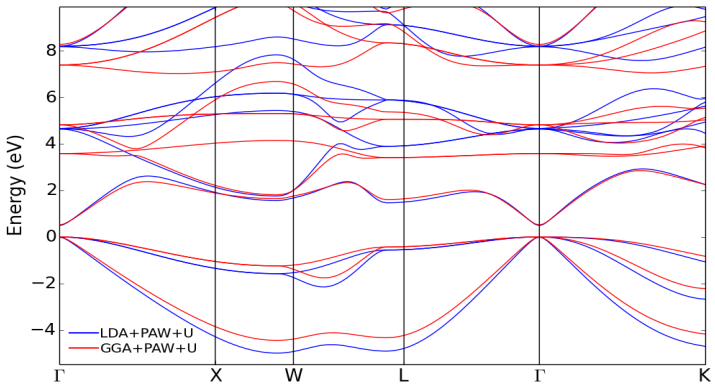

Figure 2.2: InAs band structure calculated by JTH-LDA and PBE PAW pseudopotentials within "U correction" (without spin-orbit interaction).

Table 2.8: The values used in our calculations for InAs to fit our computational results to the experimental data.

Property	JTH-LDA PAW	JTH-PBE PAW
U (eV)	13.5	15.5
E_{gap}(eV)	0.42	0.42
$k-grid$	6×6×6	6×6×6
E_{cutoff} (eV)	680	680

"U" parameter in the existence of spin-orbit coupling was taken to be a rather high value ~ 45 eV in order to achieve the required band gap. Is such a U value physically justifiable? Can we assume the U parameter to be strain independent? With these concerns, we concluded that PAW+U method is not satisfactory although the desired results due to this adjustable parameter can be obtained. Can the hybrid functionals provide a more robust and reliable alternative?

2.2.2 Hybrid Functionals

Hybrid functionals basically combine LDA or GGA exchange-correlation functionals with Hartree-Fock (exact) exchange and they are applied with the generalized KS equation. HF term in the KS leads us to non-local exchange potential in one-particle equation. Recently, the most popular hybrid functionals are as follows: PBE0 [52], PBE [53, 54], HSE (Heyd-Scuseria-Ernzerhof) [55], HSE03 [56], HSE06 [57], PBEsol [43, 44] and HSEsol [45]. We have chosen HSEsol functional since it has been shown that it gives satisfying results for small gap semiconductors. Due to the fact that the calculation of long-range (LR) part of HF (exact) term for localized basis sets (PAW) is troublesome and computationally costly, HSE have used conventional local functional, while for the short-range (SR) part, a non-local HF form is retained. With this target, Coulomb potential is divided into two parts which include (Complementary) Error functions

$$V(r,r') = \underbrace{\frac{\texttt{Erf}(\omega|r-r'|)}{|r-r'|}}_{V^{LR}} + \underbrace{\frac{\texttt{Erfc}(\omega|r-r'|)}{|r-r'|}}_{V^{SR}}. \tag{2.12}$$

In other words, HSE proposed a new hybrid functional which possesses the exact exchange mixing only for short range interactions in both HF and DFT (LDA, GGA or PBE). Hence, computational cost has been decreased. Non-local HF exchange-correlation potential is;

$$\begin{aligned} V_{xc}(r,r') &= \beta V_x^{SR,exact}(r,r';\omega) + \alpha V_x^{LR,exact}(r,r';\omega) \\ &+ (1-\beta)V_x^{SR}(r,r';\omega) + (1-\alpha)V_x^{LR}(r,r';\omega) + V_c(r). \end{aligned} \tag{2.13}$$

α and β parameters represent the contributions of LR and SR exchange parts [58]. SR,exact and LR,exact labelled potentials are non-local HF potentials while SR and LR labelled ones represent only local or semi-local based functional exchange potentials. HSEsol functional method [45] is based on solving Eq. (2.13) in the case of $\alpha = 0$ and $\beta = 0.25$. The energy expression acquired from Eq. (2.13);

$$E_{xc}^{HSEsol} = \frac{1}{4}E_x^{SR,exact} + \frac{3}{4}E_x^{SR,PBEsol} + E_x^{LR,PBEsol} + E_c^{PBEsol}\ . \tag{2.14}$$

HSEsol functional is indeed based on HSE06 functional which has the same form and range-separation parameter $\omega = 0.207$ Å^{-1}. The only difference between

them is usage of the functional for the local part which PBEsol is used as semi-local part in HSEsol functional instead of PBE in HSE06. Basically, PBE and PBEsol functionals have the same form as GGA types except their μ parameter in the density gradient expansion (GE) for the exchange part ($\mu_x^{PBE} = 2\mu_x^{PBEsol} = 2\mu_x^{GE}$) [59]. PBEsol restores the GE as $\mu_x^{PBEsol} = \mu_x^{GE}$ since in PBE functionals, GE coefficient is twice of HF (exact) one that always causes an overestimation in the lattice parameters.

The obtained energy band gap from one-electron energy of only local or semi-local functionals are very small compared to the experimental results, while contribution of non-local exchange energy (see Eq. (2.14)) plausibly increases the band gap energies in quite good agreement with the experimental results (see Table 2.9).

Table 2.9: Comparison of our calculations and experimental results. Δ_0 and a_{gap} represent the spin-orbit splitting and hydrostatic deformation potential at Γ point, respectively.

	GaAs		InAs		GaSb		InSb	
Property	HSEsol	Expt.[a]	HSEsol	Expt.[a]	HSEsol	Expt.[a]	HSEsol	Expt.[a]
E_{gap} (eV)	1.36	1.52	0.34	0.42	0.81	0.81	0.27	0.23
a_{gap} (eV)	-8.69	-8.3	-5.95	-5.7	-8.44	-8.3	-6.67	-6.08
Δ_0 (eV)	0.36	0.34	0.38	0.39	0.72	0.76	0.76	0.81

We have used the PAW pseudopotentials where d orbitals are taken as valence for cations, and conventional ones for anions in the hybrid calculations.
[a] Reference [60]

Table 2.10: Cutoff energy and k-grid values used in our VASP and ABINIT calculations.

	VASP	ABINIT
E_{cutoff} (eV)	450	680
$k-grid$	4×4×4	6×6×6

Hybrid calculations are performed by "Vienna Ab-initio Simulation Package" (VASP) [61] due to limited implementations of hybrid functionals on ABINIT.

We have given the used k-grid and cutoff energies in our calculations by ABINIT and VASP code with the Table (2.10).

Chapter 3

How Strain Affects the Electronic Band Structure

Response of semiconductors to external force is determined by their elastic properties. Stress is described as an applied external force on a certain area and the normalized geometric distortion is known as strain [62]. In other words, strain is structural unit deformation while stress is a force per unit area.

$$\begin{aligned} \varepsilon_{ij} &= S_{ijkl} X_{kl}, \\ X_{ij} &= C_{ijkl} \varepsilon_{kl}, \\ \nu &= -\frac{\varepsilon_{\perp}}{\varepsilon_{\parallel}}, \end{aligned}$$

where S_{ijkl} and C_{ijkl} are compliances and stiffness tensors, respectively. ε represents strain tensor, while X denotes stress tensor. ν is Poission's ratio, $\varepsilon_{\perp}$ and $\varepsilon_{\parallel}$ represent strain components perpendicular and parallel to the interface. S_{ijkl} and C_{ijkl} are fourth rank tensors which have total 81 components. By symmetry of the crystal structure, the number of independent constants of aforementioned tensors reduce from 81 to 36 components. Also, the symmetry of S_{ijkl} and C_{ijkl} in the first two and the last two suffixes makes it possible to use the matrix notation. Both are written with a single suffix running from 1 to 6.

3.1 Specific Strains

Strain may be generated in various ways:

- A semiconductor may be exposed to a hydrostatic pressure to cause a strain, in which case the cubic unit cell is strained compressive or tensile uniformly in all three directions. Hydrostatic strain shows its fingerprint on the band structure as a rigid shift as shown in the Figure (3.1).

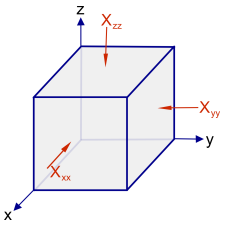

$$X_{hyd} = \begin{bmatrix} X & 0 & 0 \\ 0 & X & 0 \\ 0 & 0 & X \end{bmatrix}, \quad \varepsilon_{hyd} = (S_{11} + 2S_{12})X \begin{bmatrix} 1 & 0 & 0 \\ 0 & 1 & 0 \\ 0 & 0 & 1 \end{bmatrix} .$$

$$\varepsilon_{xx} = \varepsilon_{yy} = \varepsilon_{zz} = (S_{11} + 2S_{12})X \, . \tag{3.1}$$

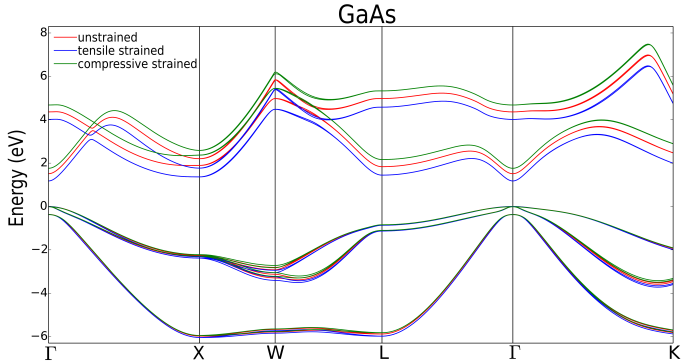

Figure 3.1: Band structure of unstrained, hydrostatically compressive and tensile strained GaAs calculated by HSEsol hybrid functional. The band gap energy goes up with the hydrostatic compressive stress and decreases by the hydrostatic tensile stress. Note that valence band maxima in all cases are set as energy references.

- Another way is to subject to a uniaxial stress along just one axis (e.g. z), while the perpendicular surfaces to the other two axes remain free, which

usually results in tensile strain along x and y in reaction to compressive stress along z.

Suppose that there is a uniaxial stress along [001] direction (equivalent to z-direction), then the strain tensors in cubic crystals can be written in terms of stress tensors:

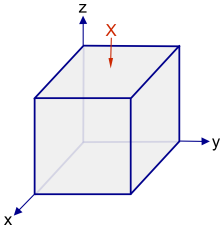

$$X_{001} = \begin{bmatrix} 0 & 0 & 0 \\ 0 & 0 & 0 \\ 0 & 0 & X \end{bmatrix}, \quad \varepsilon_{001} = \begin{bmatrix} S_{12}X & 0 & 0 \\ 0 & S_{12}X & 0 \\ 0 & 0 & S_{11}X \end{bmatrix} \tag{3.2}$$

Uniaxial stress along [111], in other words body diagonally stressed, requires two rotational transformations. After the transformation, the stress and strain tensors become:

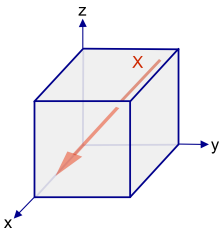

$$X_{111} = \frac{X}{3}\begin{bmatrix} 1 & 1 & 1 \\ 1 & 1 & 1 \\ 1 & 1 & 1 \end{bmatrix},$$

$$\varepsilon_{111} = \begin{bmatrix} \frac{X}{3}(S_{11}+2S_{12}) & \frac{S_{44}}{6}X & \frac{S_{44}}{6}X \\ \frac{S_{44}}{6}X & \frac{X}{3}(S_{11}+2S_{12}) & \frac{S_{44}}{6}X \\ \frac{S_{44}}{6}X & \frac{S_{44}}{6}X & \frac{X}{3}(S_{11}+2S_{12}) \end{bmatrix}. \tag{3.3}$$

- Another practical case is to apply biaxial pressure along two axes (e.g. x and y) while remaining the other one axis free. Hence, one ends up with compressive stress along x and y axes while tensile strain along z.

  Analyzing biaxial stress along [001], one achieves the following stress tensor matrix and strain tensors in terms of stress components by supposing that the magnitude of the biaxial stress is not uniform. Defining the magnitude of the force per unit area in X_{xx} and in X_{yy} direction;

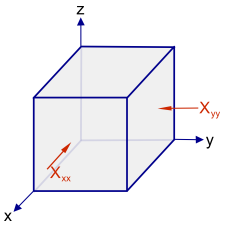

$$X_{001} = \begin{bmatrix} X_{xx} & 0 & 0 \\ 0 & X_{yy} & 0 \\ 0 & 0 & 0 \end{bmatrix}$$

$$\varepsilon_{001} = \begin{bmatrix} S_{11}X_{xx} + S_{12}X_{yy} & 0 & 0 \\ 0 & S_{11}X_{yy} + S_{12}X_{xx} & 0 \\ 0 & 0 & S_{12}(X_{xx} + X_{yy}) \end{bmatrix} .$$

In case of the uniform biaxial stress along [001] (i.e. $X_{xx} = X_{yy} = X$), the strain tensors become:

$$\begin{aligned} \varepsilon_{xx} &= (S_{11} + S_{12})X, \\ \varepsilon_{yy} &= (S_{11} + S_{12})X, \\ \varepsilon_{zz} &= 2S_{12}X \, . \end{aligned}$$

As for biaxial stress along [111], we can use the rotational invariant property of the cubic crystal. In this case, we should take the rotational transformation twice about one axis. In our case, it is z-axis of the original coordinate system and y-axis of the first rotated coordinate system. According to that procedure, the final expressions for the strain tensors in the original system become:

$$X_{111} = \frac{1}{3} \begin{bmatrix} X_{xx}/2 + X_{yy}/6 & -X_{xx}/2 + X_{yy}/6 & -X_{yy}/3 \\ -X_{xx}/2 + X_2/6 & X_{xx}/2 + X_2/6 & -X_{yy}/3 \\ -X_{yy}/3 & X_{yy}/3 & 2X_{yy}/3 \end{bmatrix},$$

$$\begin{aligned} \varepsilon_{xx} &= \varepsilon_{yy} = S_{11}\left(\frac{X_{yy}}{2} + \frac{X_{zz}}{6}\right) + S_{12}\left(\frac{X_{yy}}{2} + \frac{X_{zz}}{6}\right) + S_{12}\frac{2X_{zz}}{3}, \\ \varepsilon_{zz} &= 2S_{12}\left(\frac{X_{yy}}{2} + \frac{X_{zz}}{6}\right) + S_{11}\frac{2X_{zz}}{3}, \\ \varepsilon_{yz} &= \varepsilon_{zx} = -S_{44}\frac{X_{zz}}{6}, \\ \varepsilon_{xy} &= \frac{S_{44}}{2}\left(\frac{X_{zz}}{6} - \frac{X_{yy}}{2}\right) \, . \end{aligned}$$

If the biaxial stress along (111) is uniform (i.e. $X_{yy} = X_{zz} = X$), the expressions become:

$$\begin{aligned} \varepsilon_{xx} &= \varepsilon_{yy} = \varepsilon_{zz} = \left[\frac{2}{3}S_{11} + \frac{4}{3}S_{12}\right] X, \\ \varepsilon_{xy} &= \varepsilon_{yz} = \varepsilon_{zx} = -\frac{S_{44}}{6}X \, . \end{aligned}$$

- As yet another practical way of creating strain on a semiconductor, an epitaxial lattice mismatched layer may be grown by taking into two substrates that have different lattice constants account. This layer is compelled to get the in-plane lattice constant of the substrate and then the lattice constant of perpendicular one will be altered as well [49].

3.2 Deformation Potentials a_{gap}, b and d

Such deformations in a crystal amend the electronic energies at the different points in the Brillouin zone and the description of these changes stemmed from the lattice distortions lead us to deformation potentials [46].

According to Bir and Pikus [18], the effective strain Hamiltonian for the zinc-blende semiconductors is as follows;

$$\begin{aligned} H_{PB} = a_v(\varepsilon_{xx}+\varepsilon_{yy}+\varepsilon_{zz}) &+ 3b\left[(J_x^2 - J^2/3)\varepsilon_{xx} + c.p.\right] \\ &+ \frac{6d}{\sqrt{3}}\left(\frac{1}{2}(J_xJ_y + J_yJ_x)\varepsilon_{xy} + c.p.\right), \end{aligned}$$

where, *c.p.* indicates cyclic permutations in accordance with the indices, x, y, and z. a_v is the hydrostatic deformation potential of the valence band edge while b and d represent shear deformation potentials for VBM and J is the total angular momentum operator.

Band gap deformation potential: a_{gap} deformation potential induced by hydrostatic strain can be obtained as $a_{gap} = \dfrac{\delta E}{\mathtt{Tr}(\varepsilon)}$. Here, $\delta E = (E_{gap}^{strained} - E_{gap}^{unstrained})$ is the energy band gap difference between unstrained and hydrostatically strained cases and $\mathtt{Tr}(\varepsilon) = \varepsilon_{xx} + \varepsilon_{yy} + \varepsilon_{zz}$.

Stress along [001]: If we start to examine effective strain Hamiltonian for uniaxial stress along [001], which brings us to b deformation potential, we have

already expressed the strain tensor in terms of stress in Eq. (3.2):

$$\varepsilon_{[001]} = \underbrace{\begin{bmatrix} S_{12}X & 0 & 0 \\ 0 & S_{12}X & 0 \\ 0 & 0 & S_{11}X \end{bmatrix}}$$

$$= \underbrace{(S_{11}+2S_{12})\frac{X}{3}\begin{bmatrix} 1 & 0 & 0 \\ 0 & 1 & 0 \\ 0 & 0 & 1 \end{bmatrix}}_{\textit{Contributes to the rigid shift of all valence bands}} + \underbrace{(S_{11}-S_{12})\frac{X}{3}\begin{bmatrix} -1 & 0 & 0 \\ 0 & -1 & 0 \\ 0 & 0 & 2 \end{bmatrix}}_{\textit{Contributes to the splitting of valence bands}}$$

So that, effective strain Hamiltonian becomes for the stress along [001] as follows :

$$H_{PB}(X) \;=\; a_v(S_{11}+2S_{12})X + b(S_{11}-S_{12})(J_z^2 - J^2/3)X\,.$$

Now, we can calculate the splitting within $J = 3/2$ multiplet due to [001] uniaxial stress without including the coupling $J = 1/2$ band which we will include later. $b(S_{11}-S_{12})(J_z^2 - J^2/3)X$ part does not discriminate between m_j and $-m_j$. That is why it will only cause a splitting between $m_j = \pm 1/2$ and $m_j = \pm 3/2$. So, the following matrix elements are only taken into account:

$$\begin{aligned} \left\langle \frac{3}{2}, \pm\frac{3}{2} \middle| J_z^2 \middle| \frac{3}{2}, \pm\frac{3}{2} \right\rangle &= \frac{9}{4}, \quad \left\langle \frac{3}{2}, \pm\frac{1}{2} \middle| J_z^2 \middle| \frac{3}{2}, \pm\frac{1}{2} \right\rangle = \frac{1}{4}, \\ \left\langle \frac{3}{2}, \pm\frac{3}{2} \middle| J^2 \middle| \frac{3}{2}, \pm\frac{3}{2} \right\rangle &= \left\langle \frac{3}{2}, \pm\frac{1}{2} \middle| J^2 \middle| \frac{3}{2}, \pm\frac{1}{2} \right\rangle = \frac{15}{4}, \end{aligned}$$

Then, the contribution to the splitting of valence bands comes from the following expression:

$$\begin{aligned} \left\langle \frac{3}{2}, \frac{3}{2} \middle| b(S_{11}-S_{12})(J_z^2 - J^2/3)X \middle| \frac{3}{2}, \frac{3}{2} \right\rangle &= b(S_{11}-S_{12})X, \\ \left\langle \frac{3}{2}, \frac{1}{2} \middle| b(S_{11}-S_{12})(J_z^2 - J^2/3)X \middle| \frac{3}{2}, \frac{1}{2} \right\rangle &= -b(S_{11}-S_{12})X, \end{aligned}$$

Hence, the linear strain splitting between $m_j = \pm 3/2$ and $m_j = \pm 1/2$ states under [001] stress is:

$$\delta E_{001} \;=\; 2b(S_{11}-S_{12})X = 2b(\varepsilon_{xx} - \varepsilon_{zz})\;.$$

The fingerprint of this distortion on the electronic structure is shown in the Fig. (3.2).

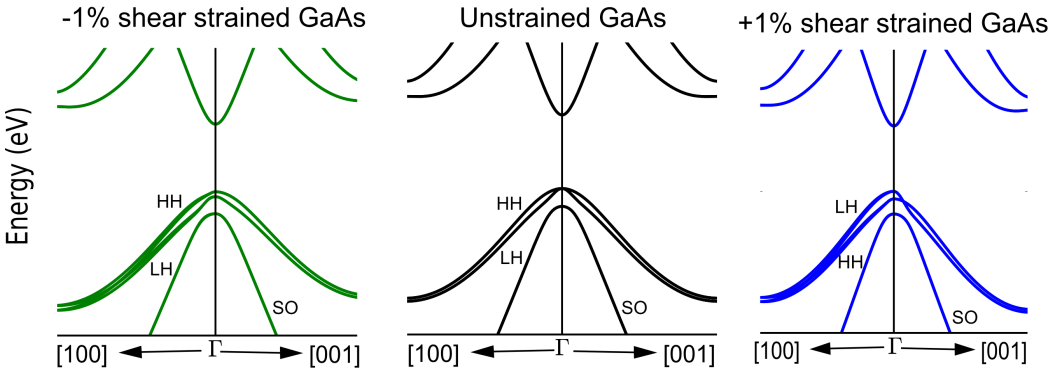

Figure 3.2: The effect of shear compression and tension stress along [001] on the electronic structure of GaAs calculated by HSEsol hybrid functionals. With this deformation, face centered cubic (FCC) cell in the unstrained case becomes a body centered tetragonal cell.

Stress along [111]: The strain components for this case, which leads to d deformation potential, has already been shown in Eq. (3.3);

$$\varepsilon_{111} = \underbrace{\begin{bmatrix} \frac{X}{3}(S_{11}+2S_{12})X & \frac{S_{44}}{6}X & \frac{S_{44}}{6}X \\ \frac{S_{44}}{6}X & \frac{X}{3}(S_{11}+2S_{12})X & \frac{S_{44}}{6}X \\ \frac{S_{44}}{6}X & \frac{S_{44}}{6}X & \frac{X}{3}(S_{11}+2S_{12})X \end{bmatrix}}$$

$$= \underbrace{(S_{11}+2S_{12})\frac{X}{3}\begin{bmatrix} 1 & 0 & 0 \\ 0 & 1 & 0 \\ 0 & 0 & 1 \end{bmatrix}}_{\textit{Contributes to the rigid shift of all valence bands}} + \underbrace{\frac{S_{44}}{6}X\begin{bmatrix} 0 & 1 & 1 \\ 1 & 0 & 1 \\ 1 & 1 & 0 \end{bmatrix}}_{\textit{Contributes to the splitting of valence bands}}$$

Hence, the effective strain Hamiltonian for stress along [111] direction can be written as follows [16]:

$$H_{PB} = a_v(S_{11}+2S_{12})X + \frac{6d}{\sqrt{3}}\left(\frac{S_{44}}{6}X\right)(\{J_xJ_y\}+\{J_yJ_z\}+\{J_zJ_x\}),$$

where curly brackets denote the symmetrized product: $\{J_xJ_y\} = \frac{1}{2}(J_xJ_y + J_yJ_x)$. So, related splitting energy can be shown as:

$$\delta E_{111} = \frac{d}{\sqrt{3}}S_{44}X = 2\sqrt{3}d\varepsilon_{xy}\ .$$

We may rotate a crystal such that [111] direction becomes the z-axis (after twice rotation). So that, the same form of the Hamiltonian matrix used for along [001] direction is also applicable along [111] direction;

$$\begin{bmatrix} -\frac{1}{3}\Delta_{SO} + \frac{1}{2}\delta E_{111} & 0 & 0 \\ 0 & -\frac{1}{3}\Delta_{SO} - \frac{1}{2}\delta E_{111} & -\frac{\sqrt{2}}{2}\delta E_{111} \\ 0 & -\frac{\sqrt{2}}{2}\delta E_{111} & \frac{2}{3}\Delta_{SO} \end{bmatrix} .$$

Diagonalizing this matrix, equations for average energies become certainly the same as stress along [001] direction and one should only replace δE_{001} by δE_{111} [46]. The behavior of the electronic structure associated with this type of deformation is shown in Fig. (3.3).

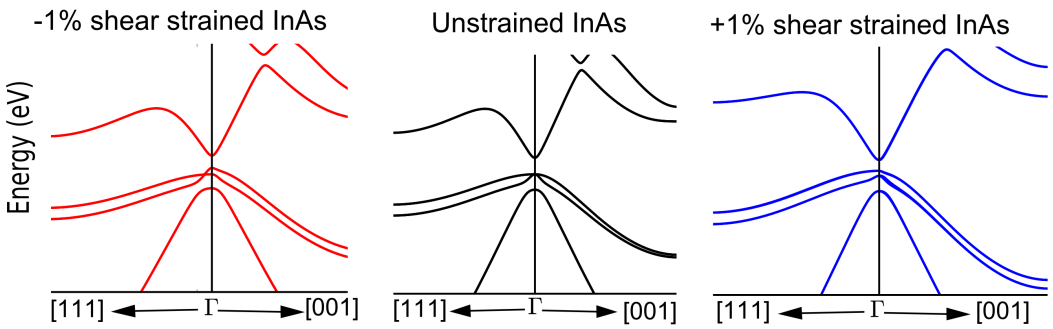

Figure 3.3: The effect of shear compression and tension stress along [111] on the electronic structure of InAs calculated by HSEsol hybrid functionals.. After uniaxial stress operation along [111], FCC structure turns into a trigonal (rhombohedral) cell with $C_{4\nu}$ space group which specifically points out ditrigonal pyramid structure.

Now, we can include $J = 1/2$ band as well. It is observed that $\left(|\frac{3}{2}, \pm\frac{3}{2}\rangle\right)$ state decouples from $\left(|\frac{3}{2}, \pm\frac{1}{2}\rangle\right)$ and $\left(|\frac{1}{2}, \pm\frac{1}{2}\rangle\right)$. Now, these two states are mixed in here due to strain.

Labeling as $V_1\left(|\frac{3}{2}, \pm\frac{1}{2}\rangle\right)$, $V_2\left(|\frac{3}{2}, \pm\frac{3}{2}\rangle\right)$, $V_3\left(|\frac{1}{2}, \pm\frac{1}{2}\rangle\right)$, we go to average energy of these bands at Γ which reflects shifts of the valence bands under uniaxial stress along [001]:

$$\begin{aligned} \Delta E_{V_2} &= \frac{1}{3}\Delta_{SO} - \frac{1}{2}\delta E_{001} , \\ \Delta E_{V_1} &= -\frac{1}{6}\Delta_{SO} + \frac{1}{4}\delta E_{001} + \frac{1}{2}\left[\Delta_{SO}^2 + \Delta_{SO}\delta E_{001} + \frac{9}{4}(\delta E_{001})^2\right]^{1/2} , \end{aligned}$$

$$\Delta E_{V_3} = -\frac{1}{6}\Delta_{SO} + \frac{1}{4}\delta E_{001} - \frac{1}{2}\left[\Delta_{SO}^2 + \Delta_{SO}\delta E_{001} + \frac{9}{4}(\delta E_{001})^2\right]^{1/2} .$$

ΔE_{V_1}, ΔE_{V_2} and ΔE_{V_3} expressions for stress along [111] have the same form the same as along [001]. One should only replace energy along [111] direction δE_{111}. Note that in the absence of spin-orbit interaction, $\Delta_{SO} = 0$.

3.2.1 Direct Lattice Vectors Under Arbitrary Strain

The unit vectors along $\hat{x}$, $\hat{y}$, $\hat{z}$ direction under strain are modified as;

$$\begin{aligned}
\mathbf{x_s} &= (1+\varepsilon_{xx})\hat{x} + \varepsilon_{xy}\hat{y} + \varepsilon_{xz}\hat{z} , \\
\mathbf{y_s} &= \varepsilon_{yx}\hat{x} + (1+\varepsilon_{yy})\hat{y} + \varepsilon_{yz}\hat{z} , \\
\mathbf{z_s} &= \varepsilon_{zx}\hat{x} + \varepsilon_{zy}\hat{y} + (1+\varepsilon_{zz})\hat{z} .
\end{aligned}$$

Then, the primitive vectors in direct space for zinc-blende crystals before and after strain become:

$$\begin{aligned}
\mathbf{a_1} &= \frac{a}{2}(\hat{y}+\hat{z}) \rightarrow \frac{a}{2}(\mathbf{y_s}+\mathbf{z_s}) , \\
\mathbf{a_2} &= \frac{a}{2}(\hat{x}+\hat{z}) \rightarrow \frac{a}{2}(\mathbf{x_s}+\mathbf{z_s}) , \\
\mathbf{a_3} &= \frac{a}{2}(\hat{x}+\hat{y}) \rightarrow \frac{a}{2}(\mathbf{x_s}+\mathbf{y_s}) .
\end{aligned}$$

Hence, strained lattice vectors in direct space for uniaxial stresses along [001] and [111] directions are given as follows;

Along [001]:

$$\begin{aligned}
\mathbf{a_{1s}} &= \frac{a}{2}[0\hat{x} + (1+\varepsilon_{yy})\hat{y} + (1+\varepsilon_{zz})\hat{z}] , \\
\mathbf{a_{2s}} &= \frac{a}{2}[(1+\varepsilon_{xx})\hat{x} + 0\hat{y} + (1+\varepsilon_{zz})\hat{z}] , \\
\mathbf{a_{3s}} &= \frac{a}{2}[(1+\varepsilon_{xx})\hat{x} + (1+\varepsilon_{yy})\hat{y} + 0\hat{z}] ,
\end{aligned}$$

Along [111]:

$$\mathbf{a_{1s}} = \frac{a}{2}[(\varepsilon_{yx}+\varepsilon_{zx})\hat{x} + (1+\varepsilon_{yy}+\varepsilon_{zy})\hat{y} + (1+\varepsilon_{zz}+\varepsilon_{yz})\hat{z}] ,$$

$$
\begin{aligned}
\mathbf{a_{2s}} &= \frac{a}{2}[(1+\varepsilon_{xx}+\varepsilon_{zx})\hat{x}+(\varepsilon_{zy}+\varepsilon_{xy})\hat{y}+(1+\varepsilon_{zz}+\varepsilon_{xz})\hat{z}] \ , \\
\mathbf{a_{3s}} &= \frac{a}{2}[(1+\varepsilon_{xx}+\varepsilon_{yx})\hat{x}+(1+\varepsilon_{yy}+\varepsilon_{xy})\hat{y}+(\varepsilon_{yz}+\varepsilon_{xz})\hat{z}] \ .
\end{aligned}
$$

In our case, we take the uniaxial stress along [111] into account to obtain "d" shear deformation potentials, which means $\varepsilon_{xx}=\varepsilon_{yy}=\varepsilon_{zz}=0$ and $\varepsilon_{xy}=\varepsilon_{yz}=\varepsilon_{zx}\neq 0$:

$$
\begin{aligned}
\mathbf{a_{1s}} &= \frac{a}{2}[(2\varepsilon_{xy})\hat{x}+(1+\varepsilon_{xy})\hat{y}+(1+\varepsilon_{xy})\hat{z}] \ , \\
\mathbf{a_{2s}} &= \frac{a}{2}[(1+\varepsilon_{xy})\hat{x}+(2\varepsilon_{xy})\hat{y}+(1+\varepsilon_{xy})\hat{z}] \ , \\
\mathbf{a_{3s}} &= \frac{a}{2}[(1+\varepsilon_{xy})\hat{x}+(1+\varepsilon_{xy})\hat{y}+(2\varepsilon_{xy})\hat{z}] \ .
\end{aligned}
$$

Strained cases in DFT hybrid calculations are imposed by the aforementioned strained lattice vectors into the VASP (see Appendix B).

3.2.2 Results

During our study associated with deformation potential parameters, we encountered significant variance, especially, in GaAs and InAs experimental parameters in the literature (see Table 3.1). Not surprisingly, there is also a wide variance between theoretical and experimental results and for some parameters, the values are reported in a range as shown in the Table 3.1. Even some 'recommended' values do not lie within those ranges! Moreover, $d/b = 2.4 \mp 0.1$ proportion of shear deformation potentials was given based on the investigations on acceptor-bound excitons in uniaxially and biaxially strained GaAs epilayers while this ratio does not exist for InAs, GaSb and InSb. According to our calculations, it is $d/b = 2.23$.

Table 3.1: Deformation potentials a_{gap}, b and d in eV units. Here, EPM values are fitted to HSEsol results under 1% strain.

Material		This Work		Literature
		EPM	HSEsol	
GaAs	a_{gap}	-8.69	-8.69	-6.5-(-20.4)[a], -8.33[d], -8.44[j], -8.76[e]
	b	-2.13	-2.13	-1.6-(-3.9)[a],-1.7[f], -1.9[h],[e], -2.0[c],[d], -2.79[h],[b]
	d	-4.77	-4.77	-2.7-(-6.0)[a], -4.23[h], [e], -4.5[c], -4.77[g],-7.5[b]
GaSb	a_{gap}	-8.44	-8.44	-8.3[a]
	b	-2.23	-2.23	-1.6[b], -1.9[f],-2.0[c],[a], -2.3[g]
	d	-5.0	-5.0	-3.98[g], -4.7[c],[a], -4.8[i], -5.0[b]
InAs	a_{gap}	-5.95	-5.95	-6.08-(-16.9)[a],
	b	-1.76	-1.76	-1.0-(-5.9)[a], -1.55[h],[e], -1.7[f],[d], -1.72[b], -1.8[c], -2.33[g]
	d	-4.25	-4.25	-8-(-2.57)[a], -3.1[h],[e], -3.3[b], -3.6[c], -3.83[g]
InSb	a_{gap}	-6.67	-6.67	-7.2[a]
	b	-1.88	-1.88	-2.0[c],[g],[a], -2.3[b]
	d	-4.62	-4.62	-4.7[a] , -4.8[c], -5.2[b]

[a]Ref. [5] [e]Ref. [30] [i]Ref. [63]
[b]Ref. [3] [f]Ref. [29] [j]Ref. [25]
[c]Ref. [19] [g]Ref. [28]
[d]Ref. [1] [h]Ref. [20]

Table 3.2: Comparison of the experimental and theoretical data in the literature with our calculations. E_{gap} represents direct energy gap (eV). Δ_0 represents spin-orbit splitting (eV) at Γ point and a_0 is the lattice constant (Å)
.

		This Work		Expt.[a]
Material		EPM	HSEsol	
GaAs	E_{gap}	1.36	1.51	1.52
	Δ_0	0.36	0.36	0.32-0.36
	a_0	5.653	5.626	5.653
GaSb	E_{gap}	0.81	0.81	0.811-0.813
	Δ_0	0.72	0.72	0.749-0.82
	a_0	6.095	6.059	6.059
InAs	E_{gap}	0.34	0.41	0.41-0.45
	Δ_0	0.38	0.38	0.37-0.41
	a_0	6.058	6.043	6.058
InSb	E_{gap}	0.27	0.23	0.235
	Δ_0	0.76	0.76	0.8-0.9
	a_0	6.479	6.457	6.479

[a] Ref. [5]

As we mentioned in the previous section, there are two special strain components each associated with its own deformation potentials: Hydrostatic strain that shifts the energies of the bands due to the fractional volume change and biaxial strain which comes from the uniaxial stress that splits the degeneracy of conduction, light hole (LH) and heavy hole (HH) valence band edges (Fig. 3.1, Fig. 3.4, Fig. 3.5, Fig. 3.6, Fig. 3.7, Fig. 3.8). As expected, these deformations leave a mark on the energy band gaps and give an opportunity to tune them. Only 1% compressive hydrostatic strain causes an increase on the band gaps at the rate of 17-19% for GaAs, 43-52% for InAs, 31% for GaSb and 72-85% for InSb while shear deformations resulting from uniaxial stresses along [001] and [111] reduce the gap around the same ranges (see Table 3.3). We have noticed that the materials including In cation are much more sensitive than the ones including Ga. InAs and InSb give significant reactions for even 1% strain.

Table 3.3: Energy band gap values (in eV) under 1% compressive hydrostatic and shear strains along [001] and [111] calculated by EPM and HSEsol functional. Relevant energy gaps are denoted as E^a_{gap} , E^b_{gap} and E^d_{gap}, respectively.

		This Work	
Material		EPM	HSEsol
GaAs	E^a_{gap}	1.77	1.62
	E^b_{gap}	1.40	1.29
	E^d_{gap}	1.37	1.24
GaSb	E^a_{gap}	1.06	1.06
	E^b_{gap}	0.70	0.74
	E^d_{gap}	0.67	0.69
InAs	E^a_{gap}	0.58	0.52
	E^b_{gap}	0.35	0.28
	E^d_{gap}	0.29	0.25
InSb	E^a_{gap}	0.435	0.478
	E^b_{gap}	0.18	0.21
	E^d_{gap}	0.12	0.18

In the Fig. (3.4), for -1% deformed case (left), a crossing is observed along the applied stress direction, which stands for, HH and LH exchange their spot. Likewise, switching of HH and LH characteristics appears in InAs, GaSb and InSb as indicated in the following figures, Fig. (3.5), Fig. (3.6), Fig. (3.7).

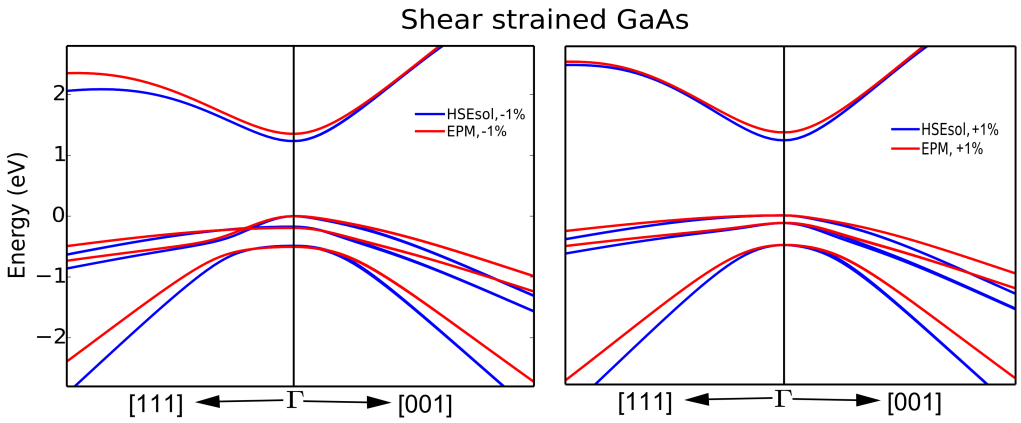

Figure 3.4: Comparison of EPM and HSEsol calculations for uniaxial stressed GaAs along [111] ($\mp 1\%$ "d").

The same behavior as we have met in biaxial strain along [111] (-1%) occurs via the application of biaxially tensile strain (+1%) to the crystal along [001] direction as well, shown in the Fig. 3.11c. However, the exchange of the characteristics of HH and LH bands does not happen under the uniaxial compressive stress (-1%) along [001] direction and the crystals have the HH and LH splittings only as given by the Fig. (3.8).

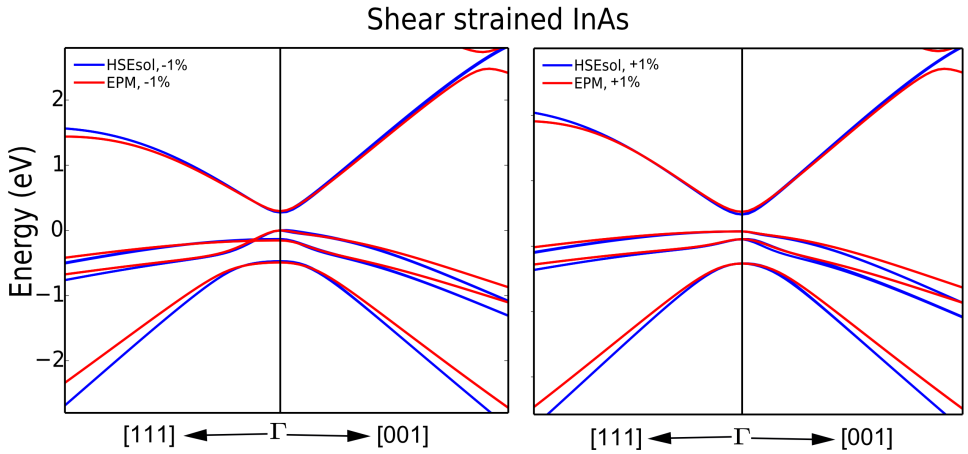

Figure 3.5: Comparison of EPM and HSEsol calculations for uniaxial stressed InAs along [111] ($\mp 1\%$ "d") d shear deformation potential is extracted under this distortion.

Also, the change of shear deformation potentials and direct band gap energies as a function of strain are displayed in Fig. 3.9 and Fig. 3.10 for GaAs and GaSb. The band gap energy variation is more or less the same under both of the shear strain cases for each material and "b" and "d" deformation potentials have a monotonous change in both $\mp$ regions.

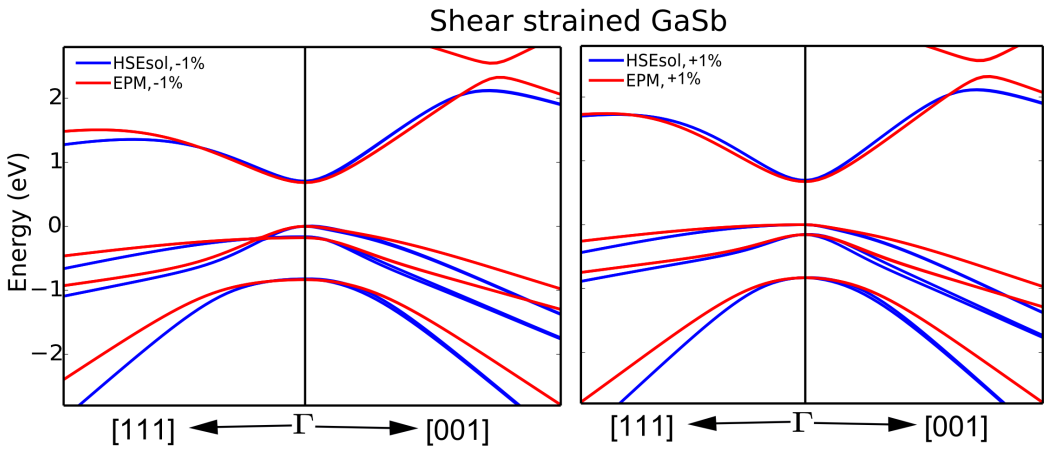

Figure 3.6: Comparison of EPM and HSEsol calculations for uniaxial stressed GaSb along [111] ($\mp 1\%$ "d") d shear deformation potential is extracted under this kind of deformation.

With this study, we have also intended to show that our EPM parametrization works not only for a couple of specific strained cases, but also for any other axial distortion, supported by HSEsol calculations as shown in the Fig. 3.11.

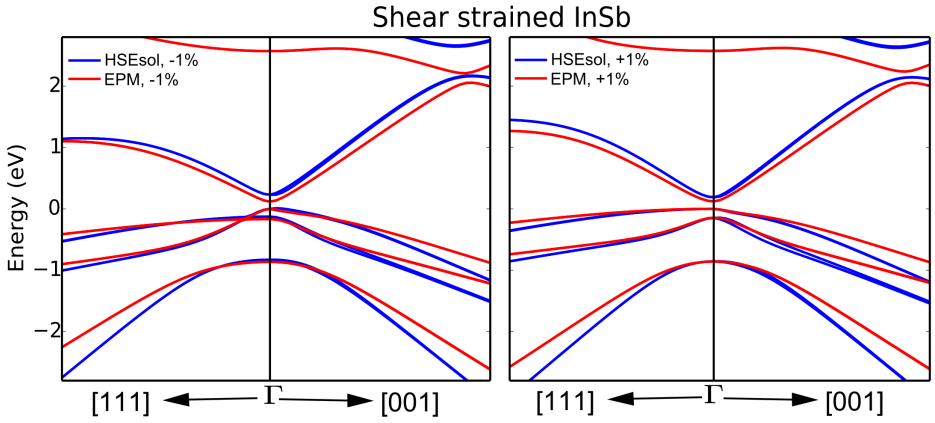

Figure 3.7: Comparison of EPM and HSEsol calculations for uniaxial stressed InSb along [111] ($\mp 1\%$ "d"). d shear deformation potential is extracted under this type of deformation.

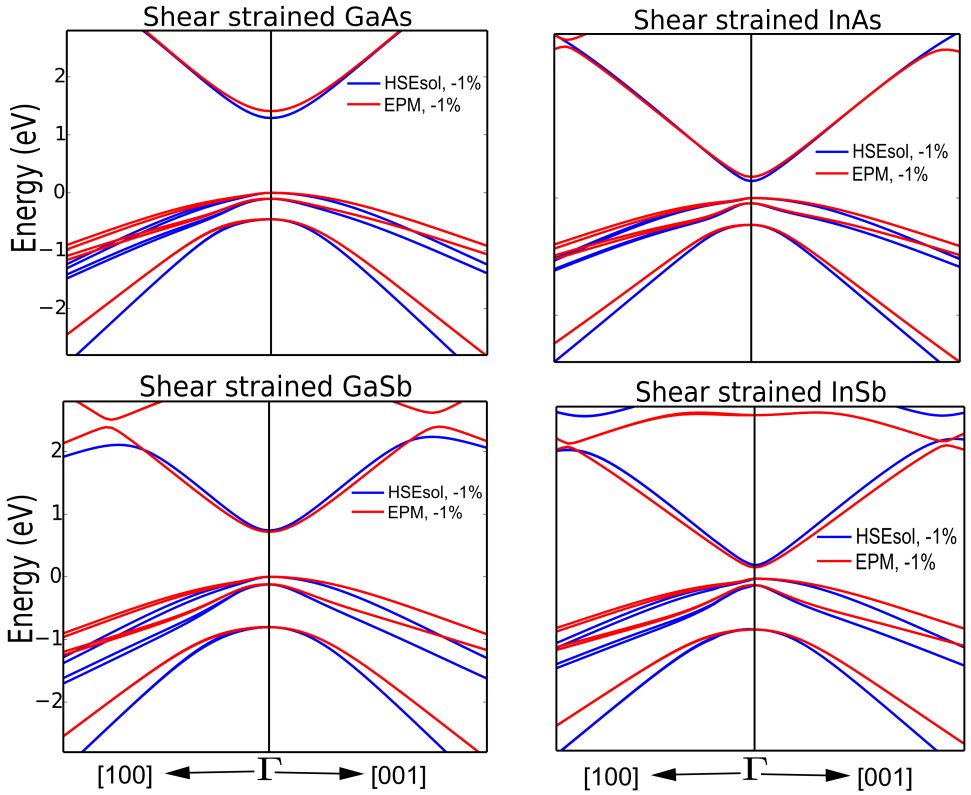

Figure 3.8: Comparison of EPM and HSEsol calculations for uniaxial stressed materials along [001] (-1% "b"). b shear deformation potential is extracted under this distortion.

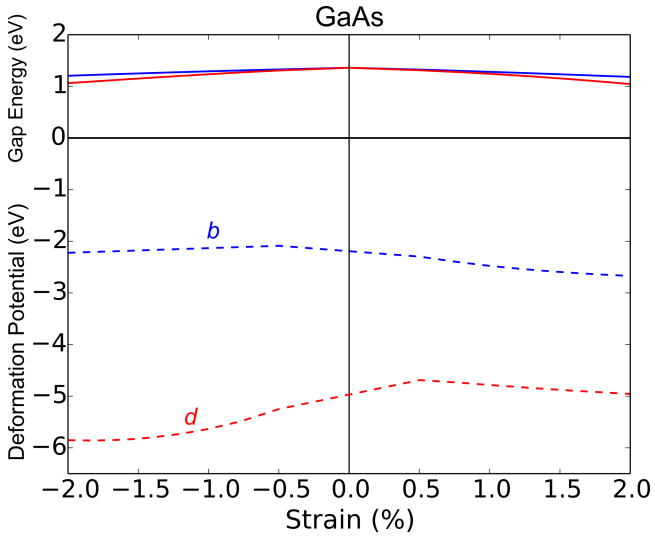

Figure 3.9: Evolution of shear deformation potentials "b" (blue dashed line) and "d" (red dashed line) and the relevant direct band gap energies (blue and red solid lines, respectively) in the range from -2% to +2% strain for GaAs calculated by HSEsol.

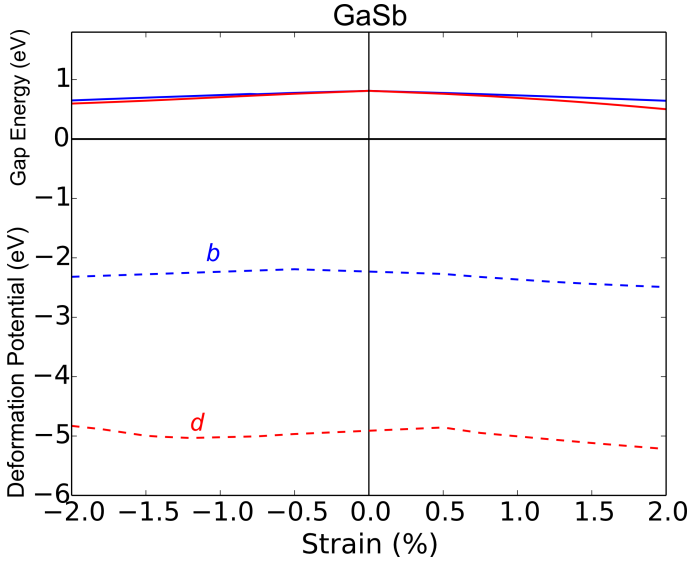

Figure 3.10: Evolution of shear deformation potentials "b" (blue dashed line) and "d" (red dashed line) and the relevant direct band gap energies (blue and red solid lines, respectively) in the range from -2% to +2% strain for GaSb calculated by HSEsol.

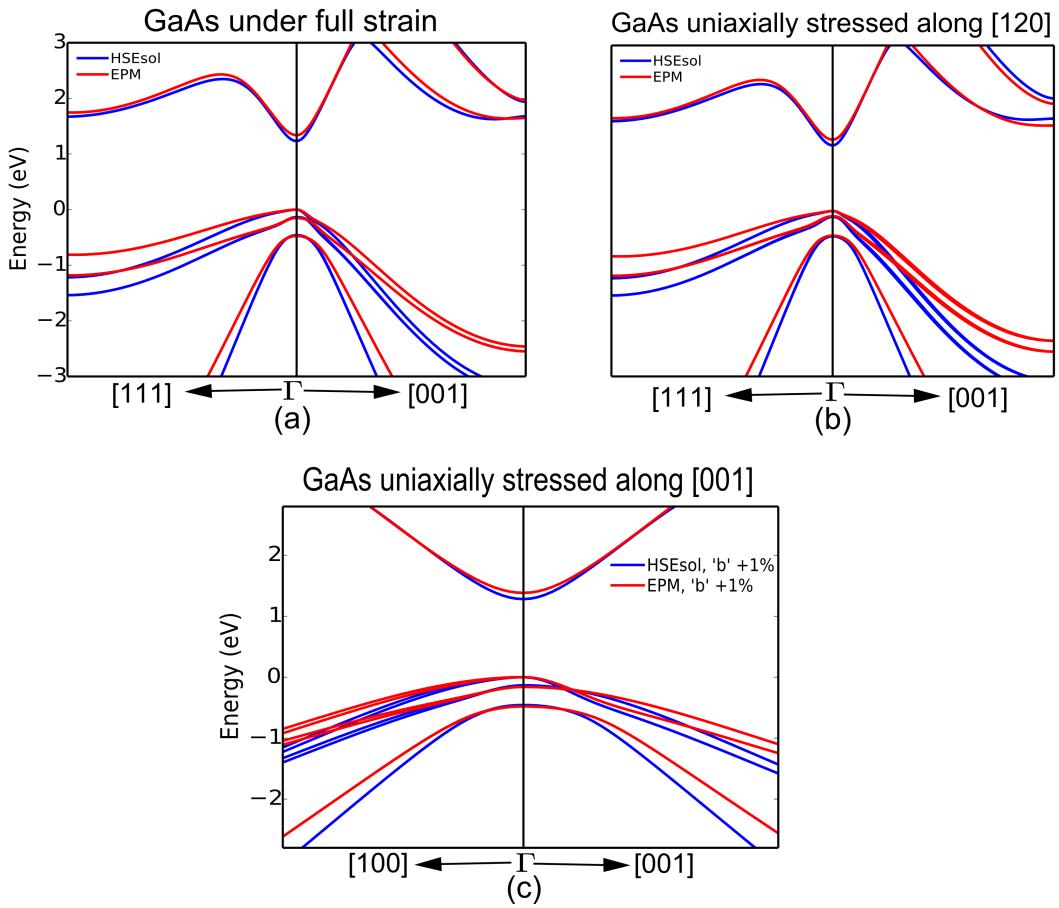

Figure 3.11: Comparison of EPM and HSEsol calculations for strained GaAs along several directions. (a): The case of GaAs under full strain which causes a triclinic cell. (b): GaAs strained along [120] direction and after that strain it becomes a monoclinic cell. (c): Biaxially tensile strained GaAs along [001], ends up with a body centered tetragonal cell. HH and LH valence bands cross and relocate along the stress direction [001].

Chapter 4

Conclusion and Outlook

Strain is generally not much welcomed within mainstream semiconductor community due to causing complexity both in theory and in growth of the QDs. However, it is demonstrated with the recent studies that it can be indeed advantageous [64, 65]. For instance, one can utilize the fact that the band structure of InAs and GaAs alter under the strain, which provides one to adjust the band gap by means of the strain according to the demand, in other words, it serves beyond the standard alloying-based the band-gap engineering paradigm. Furthermore, light hole valence bands of some semiconductors such as GaAs (as we have shown in the results section) behave as heavy hole under the biaxial tensile strain. This is highly tempting for introducing new semiconductor-based quantum systems for quantum information technologies. Particularly interesting would be to resolve how long spins endure in these states compared to their heavy hole counterparts [7]. The fact that all of the semiconductors considered in this work (GaAs, InAs, GaSb and InSb) contain 3/2, 5/2, 7/2, and 9/2 quadrupolar nuclear spins, all of them are highly prone to strain fields [66] which is ubiquitous in their low-dimensional counterparts. Therefore, strain will play an increasing role in engineering the background nuclear spin reservoir in these structures.

Within this setting of growing importance of strain, in the first part of this thesis, we have extracted the deformation potentials of GaAs, InAs, GaSb, and

InSb semiconductors using state-of-the-art hybrid density functional calculations. In lieu of this first-principles data, we have developed a new local pseudopotential parametrization having low cutoff for use in EPM-based large-scale electronic structure computations for the specific purposes of strain-modified band edges around the Γ point.

DFT electronic structures are based on HSEsol hybrid functionals using the VASP code [61, 67, 68]. For EPM, band edges of all the materials under strain obtained by the developed parametrization were fitted to HSEsol results and the strain parametrization are tabulated with the local form factors. The fingerprints of several strains on the electronic structures were demonstrated by the band structures and deformation potentials. Also, alignment of natural band offsets are incorporated based on Ref. [4] which play a crucial role in device physics.

This study characterizes especially the valence bands under arbitrary strain conditions for GaAs, InAs, GaSb and InSb to shed light on self-assembled QD studies. A natural follow-up could be the investigation of deformation potentials for the *conduction* bands. Certainly, the list of semiconductors considered in this study can also be extended towards including Group IV or heavier elements like bismuth and even thallium, thanks to new advances in hybrid DFT techniques which can supply reliable data.

Bibliography

[1] A. J. Williamson, L. W. Wang, and A. Zunger, "Theoretical interpretation of the experimental electronic structure of lens-shaped self-assembled inas/gaas quantum dots," *Phys. Rev. B*, vol. 62, pp. 12963–12977, Nov 2000.

[2] J. Wang, M. Gong, G.-C. Guo, and L. He, "Temperature dependent empirical pseudopotential theory for self-assembled quantum dots," *Journal of Physics: Condensed Matter*, vol. 24, no. 47, p. 475302, 2012.

[3] J. Kim and M. V. Fischetti, "Electronic band structure calculations for biaxially strained Si, Ge, and III-V semiconductors," *Journal of Applied Physics*, vol. 108, no. 1, 2010.

[4] Y.-H. Li, A. Walsh, S. Chen, W.-J. Yin, J.-H. Yang, J. Li, J. L. F. Da Silva, X. G. Gong, and S.-H. Wei, "Revised ab initio natural band offsets of all group IV, II-VI, and III-V semiconductors," *Applied Physics Letters*, vol. 94, no. 21, 2009.

[5] I. Vurgaftman, J. R. Meyer, and L. R. Ram-Mohan, "Band parameters for III-V compound semiconductors and their alloys," *Journal of Applied Physics*, vol. 89, no. 11, pp. 5815–5875, 2001.

[6] G. Zielinski, M. Jaskolski W. Aizpurua J. & Bryant, "Strain and spin-orbit effects in self-assembled quantum dots," *Acta Physica Polonica Series A*, vol. 108, pp. 929–940, 2005.

[7] B. G. et. al., "A light-hole exciton in a quantum dot," *Nat Phys*, vol. 10, pp. 1745–2473, 2013.

[8] E. Alphandry, R. J. Nicholas, N. J. Mason, B. Zhang, P. Mck, and G. R. Booker, "Self-assembled insb quantum dots grown on gasb: A photoluminescence, magnetoluminescence, and atomic force microscopy study," *Applied Physics Letters*, vol. 74, no. 14, 1999.

[9] E. S. Kadantsev, M. Zieliński, and P. Hawrylak, "Band engineering in nanowires: *Ab initio* model of band edges modified by (111) biaxial strain in group IIIA-VA semiconductors," *Phys. Rev. B*, vol. 86, p. 085411, Aug 2012.

[10] M. Zieliński, "Valence band offset, strain and shape effects on confined states in self-assembled InAs/InP and InAs/GaAs quantum dots," *arXiv:1303.4417*, 2013.

[11] J. Bardeen and W. Shockley, "Deformation potentials and mobilities in nonpolar crystals," *Phys. Rev.*, vol. 80, pp. 72–80, Oct 1950.

[12] C. Herring and E. Vogt, "Transport and deformation-potential theory for many-valley semiconductors with anisotropic scattering," *Phys. Rev.*, vol. 101, pp. 944–961, Feb 1956.

[13] L. J. Sham, "A calculation of deformation potentials in silicon," *Proc. Phys. Soc.*, vol. 81, Nov 1963.

[14] I. Goroff and L. Kleinman, "Deformation potentials in silicon III effects of a general strain on conduction and valence levels," *Phys. Rev.*, vol. 132, pp. 1080–1084, Nov 1963.

[15] I. Balslev, "Direct edge piezo-reflectance in Ge and GaAs," *Solid State Communications*, vol. 5, no. 4, pp. 315 – 317, 1967.

[16] F. H. Pollak and M. Cardona, "Piezo-electroreflectance in Ge, GaAs, and Si," *Phys. Rev.*, vol. 172, pp. 816–837, Aug 1968.

[17] F. H. Pollak, "Modulation spectroscopy under uniaxial stress," *Surface Science*, vol. 37, no. 0, pp. 863 – 895, 1973.

[18] G. L. Bir and P. G. E., "Symmetry and strain-induced effects in semiconductors," *Wiley, New York*, 1974.

[19] "O. Landolt-Bornstein, madelung: Numerical data and functional relationships in science and technology," *Springer Berlin*, 1982.

[20] C. G. Van de Walle, "Band lineups and deformation potentials in the model-solid theory," *Phys. Rev. B*, vol. 39, pp. 1871–1883, Jan 1989.

[21] C. G. Van de Walle and R. M. Martin, "Absolute deformation potentials: Formulation and *ab initio* calculations for semiconductors," *Phys. Rev. Lett.*, vol. 62, pp. 2028–2031, Apr 1989.

[22] S.-H. Wei and A. Zunger, "Predicted band-gap pressure coefficients of all diamond and zinc-blende semiconductors: Chemical trends," *Phys. Rev. B*, vol. 60, pp. 5404–5411, Aug 1999.

[23] Y.-H. Li, X. G. Gong, and S.-H. Wei, "Ab initio calculation of hydrostatic absolute deformation potential of semiconductors," *Applied Physics Letters*, vol. 88, no. 4, 2006.

[24] Y.-H. Li, X. G. Gong, and S.-H. Wei, "*Ab initio* all-electron calculation of absolute volume deformation potentials of IV, VI, III-V, and II-VI semiconductors: The chemical trends," *Phys. Rev. B*, vol. 73, p. 245206, Jun 2006.

[25] T. Cheiwchanchamnangij and W. R. L. Lambrecht, "Band structure parameters of wurtzite and zinc-blende GaAs under strain in the GW approximation," *Phys. Rev. B*, vol. 84, p. 035203, Jul 2011.

[26] J. R. Cárdenas and G. Bester, "Atomic effective pseudopotentials for semiconductors," *Phys. Rev. B*, vol. 86, p. 115332, Sep 2012.

[27] A. Blacha, H. Presting, and M. Cardona, "Deformation potentials of k = 0 states of tetrahedral semiconductors," *Phys. stat. sol. (b)*, vol. 126, no. 1, pp. 11–36, 1984.

[28] C. Priester, G. Allan, and M. Lannoo, "Band-edge deformation potentials in a tight-binding framework," *Phys. Rev. B*, vol. 37, pp. 8519–8522, May 1988.

[29] M. Silver, W. Batty, A. Ghiti, and E. P. O'Reilly, "Strain-induced valence-subband splitting in III-V semiconductors," *Phys. Rev. B*, vol. 46, pp. 6781–6788, Sep 1992.

[30] Y. M. Niquet, "Electronic and optical properties of InAs/GaAs nanowire superlattices," *Phys. Rev. B*, vol. 74, p. 155304, Oct 2006.

[31] R. M. Martin, "Electronic structure: Basic theory and practical methods," *Cambridge*, 2004.

[32] M. Cardona and N. E. Christensen, "Acoustic deformation potentials and heterostructure band offsets in semiconductors," *Phys. Rev. B*, vol. 35, pp. 6182–6194, Apr 1987.

[33] E. P. O'Reilly, "Axial-strain effects on superlattice band structures," *Semicond. Sci. Technol.*, vol. 1, 1986.

[34] L.-W. Wang, S.-H. Wei, T. Mattila, A. Zunger, I. Vurgaftman, and J. R. Meyer, "Multiband coupling and electronic structure of $(InAs)_n/(GaSb)_n$ superlattices," *Phys. Rev. B*, vol. 60, pp. 5590–5596, Aug 1999.

[35] M. L. Cohen, "Nanotubes, nanoscience, and nanotechnology," *Materials Science and Engineering: C*, vol. 15, no. 12, pp. 1 – 11, 2001. International Conference on Electronic Materials & European Materials Research Society, Spring Meeting, Symposium E: Current Trends in Nanotechnologies.

[36] M. L. Cohen, "Pseudopotentials and total energy calculations," *Physica Scripta T1*, vol. 5, 1982.

[37] P. J. R. C. P. Professor Marvin L. Cohen PhD, "Electronic structure and optical properties of semiconductors," *Springer Series in Solid-State Sciences*, vol. Volume 75, 1988.

[38] K. Hummer, J. Harl, and G. Kresse, "Heyd-scuseria-ernzerhof hybrid functional for calculating the lattice dynamics of semiconductors," *Phys. Rev. B*, vol. 80, p. 115205, Sep 2009.

[39] Q. Yan, P. Rinke, M. Scheffler, and C. G. Van de Walle, "Role of strain in polarization switching in semipolar InGaN/GaN quantum wells," *Applied Physics Letters*, vol. 97, no. 18, 2010.

[40] Q. Yan, P. Rinke, M. Winkelnkemper, A. Qteish, D. Bimberg, M. Scheffler, and C. G. V. de Walle, "Band parameters and strain effects in ZnO and group-III nitrides," *Semiconductor Science and Technology*, vol. 26, no. 1, p. 014037, 2011.

[41] C. Hajlaoui, L. Pedesseau, F. Raouafi, F. B. CheikhLarbi, J. Even, and J.-M. Jancu, "First-principles density functional theory study of strained wurtzite inp and inas," *Journal of Physics D: Applied Physics*, vol. 46, no. 50, p. 505106, 2013.

[42] A. Castellanos-Gomez, "Black phosphorus: narrow gap, wide applications," *arXiv:1508.00874*, 2015.

[43] J. P. Perdew, A. Ruzsinszky, G. I. Csonka, O. A. Vydrov, G. E. Scuseria, L. A. Constantin, X. Zhou, and K. Burke, "Restoring the density-gradient expansion for exchange in solids and surfaces," *Phys. Rev. Lett.*, vol. 100, p. 136406, Apr 2008.

[44] J. P. Perdew, A. Ruzsinszky, G. I. Csonka, O. A. Vydrov, G. E. Scuseria, L. A. Constantin, X. Zhou, and K. Burke, "Erratum: Restoring the density-gradient expansion for exchange in solids and surfaces [phys. rev. lett. **100** , 136406 (2008)]," *Phys. Rev. Lett.*, vol. 102, p. 039902, Jan 2009.

[45] L. Schimka, J. Harl, and G. Kresse, "Improved hybrid functional for solids: The hsesol functional," *The Journal of Chemical Physics*, vol. 134, no. 2, 2011.

[46] P. Yu and M. Cardona, "Fundamentals of semiconductors, physics and materials properties," *Springer*, 2005.

[47] J. R. Chelikowsky and M. L. Cohen, "Electronic structure of silicon," *Phys. Rev. B*, vol. 10, pp. 5095–5107, Dec 1974.

[48] J. R. Chelikowsky and M. L. Cohen, "Nonlocal pseudopotential calculations for the electronic structure of eleven diamond and zinc-blende semiconductors," *Phys. Rev. B*, vol. 14, pp. 556–582, Jul 1976.

[49] P. Harrison, "Quantum wells, wires, dots," *Wiley*, 2009.

[50] X. Gonze, B. Amadon, P.-M. Anglade, J.-M. Beuken, F. Bottin, P. Boulanger, F. Bruneval, D. Caliste, R. Caracas, M. Ct, T. Deutsch, L. Genovese, P. Ghosez, M. Giantomassi, S. Goedecker, D. Hamann, P. Hermet, F. Jollet, G. Jomard, S. Leroux, M. Mancini, S. Mazevet, M. Oliveira, G. Onida, Y. Pouillon, T. Rangel, G.-M. Rignanese, D. Sangalli, R. Shaltaf, M. Torrent, M. Verstraete, G. Zerah, and J. Zwanziger, "www.abinit.org, abinit: First-principles approach to material and nanosystem properties," *Computer Physics Communications*, vol. 180, no. 12, pp. 2582 – 2615, 2009.

[51] F. Jollet, M. Torrent, and N. Holzwarth, "Generation of projector augmented-wave atomic data: A 71 element validated table in the {XML} format," *Computer Physics Communications*, vol. 185, no. 4, pp. 1246 – 1254, 2014.

[52] C. Adamo and V. Barone, "Toward reliable density functional methods without adjustable parameters: The PBE0 model," *The Journal of Chemical Physics*, vol. 110, no. 13, 1999.

[53] J. P. Perdew, K. Burke, and M. Ernzerhof, "Generalized gradient approximation made simple," *Phys. Rev. Lett.*, vol. 77, pp. 3865–3868, Oct 1996.

[54] J. P. Perdew, K. Burke, and M. Ernzerhof, "Generalized gradient approximation made simple [phys. rev. lett. 77, 3865 (1996)]," *Phys. Rev. Lett.*, vol. 78, pp. 1396–1396, Feb 1997.

[55] J. Heyd, G. E. Scuseria, and M. Ernzerhof, "Hybrid functionals based on a screened coulomb potential," *The Journal of Chemical Physics*, vol. 118, no. 18, pp. 8207–8215, 2003.

[56] J. Heyd, G. E. Scuseria, and M. Ernzerhof, "Erratum: hybrid functionals based on a screened coulomb potential [j. chem. phys.118, 8207 (2003)]," *The Journal of Chemical Physics*, vol. 124, no. 21, 2006.

[57] A. V. Krukau, O. A. Vydrov, A. F. Izmaylov, and G. E. Scuseria, "Influence of the exchange screening parameter on the performance of screened hybrid functionals," *The Journal of Chemical Physics*, vol. 125, no. 22, 2006.

[58] A. S. Petr A. Khomyakov, Mathieu Luisier, "Compositional bowing of band energies and their deformation potentials in strained InGaAs ternary alloys: a first-principles study," *arXiv:1505.05659*, 2015.

[59] P. Haas, F. Tran, P. Blaha, K. Schwarz, and R. Laskowski, "Insight into the performance of gga functionals for solid-state calculations," *Phys. Rev. B*, vol. 80, p. 195109, Nov 2009.

[60] "Landolt and borstein, numerical data and functional relationshipsin science and technology," *Springer Berlin*, vol. 22, 1997.

[61] G. Kresse and J. Hafner, "*Ab initio* molecular dynamics for liquid metals," *Phys. Rev. B*, vol. 47, pp. 558–561, Jan 1993.

[62] T. M. C.K. Maiti, "Strain-engineered mosfets," *CRC Press*, 2012.

[63] R. A. Noack, W. Rühle, and T. N. Morgan, "Bound excitons at doubly ionizable acceptors in GaSb," *Phys. Rev. B*, vol. 18, pp. 6944–6956, Dec 1978.

[64] Y. S. J. Eric R. Hedin, "Spintronics in nanoscale devices," *CRC Press*, pp. 121–153, Aug 2013.

[65] D. Gammon, "Quantum dots: Strain is a problem no more," *Nat Nano*, vol. 7, Oct 2012.

[66] C. Bulutay, "Quadrupolar spectra of nuclear spins in strained $\mathrm{in}_x\mathrm{ga}_{1-x}\mathrm{as}$ quantum dots," *Phys. Rev. B*, vol. 85, p. 115313, Mar 2012.

[67] G. Kresse and J. Hafner, "*Ab initio* molecular-dynamics simulation of the liquid-metal amorphous-semiconductor transition in germanium," *Phys. Rev. B*, vol. 49, pp. 14251–14269, May 1994.

[68] G. Kresse and J. Furthmuller, "Efficiency of ab-initio total energy calculations for metals and semiconductors using a plane-wave basis set," *Computational Materials Science*, vol. 6, no. 1, pp. 15 – 50, 1996.

[69] M. S. Hybertsen and S. G. Louie, "Spin-orbit splitting in semiconductors and insulators from the *ab initio* pseudopotential," *Phys. Rev. B*, vol. 34, pp. 2920–2922, Aug 1986.

[70] G. Weisz, "Band structure and fermi surface of white tin," *Phys. Rev.*, vol. 149, pp. 504–518, Sep 1966.

Appendix A

Spin-orbit Interaction within Pseudopotential Framework

Following Hybertson-Luie [69], we use $\lambda \mathbf{l} \cdot \mathbf{S}$ type spin-orbit Hamiltonian;

$$\begin{aligned}
\hat{H}^{SOI} &= \frac{\hbar}{4m^2c^2} \nabla V \times \mathbf{p} \cdot \sigma, \quad \mathbf{S} = \frac{\hbar}{2}\sigma, \\
\hat{H}^{SOI} &= \frac{1}{2m^2c^2} \nabla V \times \mathbf{p} \cdot \mathbf{S} \simeq \frac{1}{2m^2c^2} \frac{1}{r} \frac{dV}{dr} \mathbf{r} \times \mathbf{p} \cdot \mathbf{S}, \\
\hat{H}^{SOI} &= \sum_{l=1}^{\infty} |l\rangle V_{so,l}(r)\ \mathbf{l}\ \sigma \langle l| \ .
\end{aligned}$$

Here, $\mathbf{S}$ is the electron spin operator, $\mathbf{l}$ is the orbital angular momentum operator and σ is the Pauli spin matrix. Our main assumption is that the essential part of spin orbit interaction will come from the vicinity of the nucleus so that we can treat $V(\mathbf{r})$ to be spherically symmetric, $V(\mathbf{r}) \to V(r)$, then if we replace $\mathbf{S}$ by σ and transfer the dimension of $\mathbf{l}$ into $V_{so,l}$, we make $V_{so,l}$ to have energy dimensions leaving the other quantities dimensionless. For electronic structure calculations, we need the planewave matrix elements:

$$H^{so}_{s\mathbf{K},s'\mathbf{K}'} = \langle s\mathbf{K}|\hat{H^{so}}|s'\mathbf{K}'\rangle,$$

where $\mathbf{K} = \mathbf{k} + \mathbf{G}$ and $\mathbf{K} = \mathbf{k} + \mathbf{G}'$ and *s, s'* are spin quantum labels; assuming one type of atom in the basis:

$$H^{so}_{s\mathbf{K},s'\mathbf{K}'} = \langle s|\sigma|s'\rangle \sum_{i,j} \int \frac{d^3r}{\Omega} e^{-i\mathbf{K}\mathbf{r}} \; \mathbf{1} \; V^{so}_l(|\mathbf{r} - \mathbf{R_j} - \tau_\mathbf{i}|)\hat{P}_l e^{i\mathbf{K}'\mathbf{r}},$$

Ω represents crystal volume and $\hat{P}_l$ projects to l for the origin chosen at the site $\mathbf{R_j} + \tau_\mathbf{i}$. Substituting $\Omega = N\Omega_0 = N_a\Omega_a$ and letting $\mathbf{r} - \mathbf{R_j} - \tau_\mathbf{i} \rightarrow \mathbf{r}$;

$$H^{so}_{s\mathbf{K},s'\mathbf{K}'} = \underbrace{\frac{1}{N\ N_a} \sum_{i,j} e^{-i(\mathbf{K}'-\mathbf{K}).(\mathbf{R_j}-\tau_\mathbf{i})}}_{\frac{1}{N\ N_a}\sum_{i,j} e^{-i(\mathbf{G}'').(\mathbf{R_j}-\tau_\mathbf{i})} = S(\mathbf{K}'-\mathbf{K})} \underbrace{\frac{1}{\Omega_a} \int d^3r e^{-i\mathbf{K}\mathbf{r}} \; \mathbf{1} \; V^{so}_l(r)\hat{P}_l e^{i\mathbf{K}'\mathbf{r}}}_{\mathbf{I}_l},$$

Here, N_a is number of atoms in basis, Ω_a is the volume per atom, $S(\mathbf{K}' - \mathbf{K})$ represents the structure factor of bulk crystals and $\mathbf{I}_l$ can be explicitly worked out as;

$$\mathbf{I}_l = \underbrace{4\pi(2l+1) \underbrace{\left[\int_0^\infty \frac{dr}{\Omega_a} r^2 j_l(Kr) V^{so}_l(r) j_l(K'r)\right]}_{V^{so}_l(K,K')}}_{V_{so,p}(K,K')} \underbrace{\int_0^\pi d\theta \sin\theta \int_0^{2\pi} d\phi Y_{lK} \; \mathbf{1} \; Y_{lK'}}_{\mathbf{f}_l(\alpha)}, \tag{A.1}$$

where, j_l is the spherical Bessel function and Y_{lK} is the spherical harmonics. Following the pioneering work of Weisz [70], the angular part $\mathbf{f}_l(\alpha)$ is given as

$$\mathbf{f}_l(\alpha) = -i(\hat{K} \times \hat{K}') \frac{dP_l(\cos\alpha)}{d\cos\alpha} \ ,$$

where P_l is the Legendre polynomials. Combining these pieces and retaining only $l = 1$ and 2, we obtain

$$H^{so}_{s\mathbf{K},s'\mathbf{K}'} = -i\langle s|\sigma|s'\rangle \left[12\pi \frac{\mathbf{K}\times\mathbf{K}'}{KK'} V^{so}_{l=1}(K,K') + 60\pi \frac{\mathbf{K}\times\mathbf{K}'}{KK'} \frac{\mathbf{K}\cdot\mathbf{K}'}{KK'} V^{so}_{l=2}(K,K')\right] S(\mathbf{K}'-\mathbf{K}) \ .$$

This expression exactly agrees with Eq. (6) of Ref. [69]. $V_{so,p}(K,K')$ for $l = 1$ is numerically computed for once and stored as a look-up table into a data file in our EPM calculations.

Appendix B

VASP: Some representative input files

B.0.3 Self-Consistent Calculation

B.0.3.1 First Step

- **INCAR**:

# Self Consistent Calculation step:
ISTART = 0
ICHARG = 2
#Electronic Relaxation:
ENCUT = 450
EDIFF = 1.0E-7
PREC = Accurate
ALGO = Normal
#Relaxation:
ISMEAR = 0
SIGMA = 0.05
IBRION = 2
ISIF = 3
NSW = 100
EDIFFG = -0.001
GGA_COMPAT = .FALSE.
NBANDS = 24
# SO:
LSORBIT = .TRUE.
LNONCOLLINEAR = .FALSE.
ISPIN= 1
#HSEsol:
GGA = PS
LHFCALC = .TRUE.
HFSCREEN = 0.207
PRECFOCK=Normal

KPOINTS:

4x4x4
0
G
4 4 4
0 0 0

POSCAR:

GaAs
5.6268
0.5 0.5 0.0
0.0 0.5 0.5
0.5 0.0 0.5
1 1
Selective Dynamics
Cartesian
0.05 0.05 0.05 T T T
0.3 0.3 0.3 T T T

First self-consistent (SC) step aims to relax all structure to obtain the theoretical lattice constant by taking ISIF=3 in INCAR file. Mainly, there should be four files: INCAR, KPOINTS, POSCAR (as given in the above) and POTCAR. POTCAR file contains PAW pseudopotentials (included in VASP) that can be formed according to the intended system.

B.0.3.2 Second Step

Second step is a SC calculation with the defined theoretical lattice constant in the previous step. Only difference from the first step is ISIF=2 in the INCAR file which implies only ionic relaxation. The other remain files are the same.

B.0.3.3 Third Step

- Changes in the INCAR file:
  #SC Calculation:
  ISTART = 1
  ICHARG = 2
  #No Ionic Relaxation:
  IBRION=-1
  NSW=0

- Third step is a SC calculation without relaxation (requires some changes in the INCAR file). On the other hand, IBZKPT, CONTCAR and WAVECAR files should be transferred from the second step for the third step calculation. They should be renamed as KPOINTS and POSCAR, respectively. WAVECAR stays as it is and is read during the third calculation.

B.0.4 Non Self-Consistent Calculation for Band Structure

- #Non-SC Calculation:
  ISTART = 1
  ICHARG = 11
  #No Relaxation:
  IBRION=-1
  NSW=0

- Fourth step is a non-SC calculation without relaxation (requires some changes in the INCAR file). Aforementioned procedure for the third step should be repeated.

Only KPOINTS file needs to have some additional lines for the bandstructure. Intended paths should be added as follows:
0.0 0.5 0.5 0.0
0.0 0.0 0.0 0.0
0.0 0.0 0.0 0.0
0.5 0.5 0.0 0.0

B.0.5 How to insert strain into VASP

This part is based on section 3.2.1. Strained cases are imposed on POSCAR file; for +1% strained materials along [111] and -1% strained materials along [001] as follows

- GaAs-shear +1% along [111]
  5.6268
  0.0100 0.5050 0.5050
  0.5050 0.0100 0.5050
  0.5050 0.5050 0.0100
  1 1
  Selective Dynamics
  Cartesian
  0.05 0.05 0.05 T T T
  0.3 0.3 0.3 T T T

- GaAs-shear -1% [001]
  5.6268
  0.000 0.495 0.510
  0.495 0.000 0.510
  0.495 0.495 0.000
  1 1
  Selective Dynamics
  Cartesian
  0.05 0.05 0.05 T T T
  0.3 0.3 0.3 T T T